OCS Study
BOEM 2016-019

Pressure Wave and Acoustic Properties Generated by the Explosive Removal of Offshore Structures in the Gulf of Mexico

U.S. Department of the Interior
Bureau of Ocean Energy Management
Gulf of Mexico OCS Region

BOEM
Bureau of Ocean Energy Management

OCS Study
BOEM 2016-019

Pressure Wave and Acoustic Properties Generated by the Explosive Removal of Offshore Structures in the Gulf of Mexico

Authors

MJ Barkaszi
A Frankel
JS Martin
W Poe

Prepared under BOEM Contract
M13PX00068
by
CSA Ocean Sciences, Inc
8502 SW Kansas Avenue
Stuart, Florida 34997

Published by

U.S. Department of the Interior
Bureau of Ocean Energy Management
Gulf of Mexico OCS Region

New Orleans, LA
March 2016

DISCLAIMER

This report was prepared under contract between the Bureau of Ocean Energy Management (BOEM) and CSA Ocean Sciences, Inc. This report has been technically reviewed by BOEM, and it has been approved for publication. Approval does not necessarily signify that the contents reflect the views and policies of BOEM, nor does mention of trade names or commercial products constitute endorsement or recommendation for use.

REPORT AVAILABILITY

To download a PDF file of this Gulf of Mexico OCS Region report, go to the U.S. Department of the Interior, Bureau of Ocean Energy Management, Environmental Studies Program Information System website and search on OCS Study BOEM 2016-019.

This report can be viewed at select Federal Depository Libraries. It can also be obtained from the National Technical Information Service; the contact information is below.

U.S. Department of Commerce
National Technical Information Service
5301 Shawnee Rd.
Springfield, Virginia 22312
Phone: (703) 605-6000, 1(800)553-6847
Fax: (703) 605-6900
Website: http://www.ntis.gov/

CITATION

Barkaszi, M.J., A. Frankle, J. Martin, and W. Poe. 2016. Pressure wave and acoustic properties generated by the explosive removal of offshore structures in the Gulf of Mexico. U.S. Dept. of the Interior, Bureau of Ocean Energy Management, Gulf of Mexico OCS Region, New Orleans, LA. OCS Study BOEM 2016-019. 69 p.

ACKNOWLEDGMENTS

The project described in this report was funded by the Bureau of Ocean Energy Management (BOEM) through Order No. M13PX00068. We would like to acknowledge the important contribution of different people who have been very much instrumental to the realization of this project. The people are not presented here in view of the importance of their contribution, but rather in terms of the timing of their involvement in the program. We appreciated the help and comments from the BOEM and Bureau of Safety and Environmental Enforcement (BSEE) personnel of their Headquarters office in Herndon, Virginia, particularly Lisa Algarin, Contracting Officer (CO). We acknowledge BOEM Gulf of Mexico OCS Region Contracting Officer Representative (COR), Dr. Tré Glenn, for his input during the development of the project, assistance in the field work, and valuable commenting during the writing of the report. Also, we acknowledge the field support and Contract Inspector (CI) efforts provided by Doug Peter, T.J. Broussard, and Daniel "Herb" Leedy from BSEE Gulf of Mexico OCS Region, and Mark Belter from BOEM Gulf of Mexico OCS Region. We also acknowledge the field and logistic support from Explosive Services International (ESI) and, in particular, William Poe and Jason Poe. Their coordination with, and assistance to, the study team, BSEE, and project owners ensured safe and successful operations.

Finally, we greatly appreciate and want to recognize the cooperation and essential contributions of Fieldwood Energy LLC; particularly, John Seeger, Vice-President of Decommissioning Operations, and Brandon DeWolfe, Facilities Operations Manager. Without Mr. Seeger's and Mr. DeWolfe's continuous, logistical coordination and generous support for the field measurement needs, the measurement activities described in this report would not have been possible.

CONTENTS

LIST OF FIGURES

LIST OF TABLES

ACRONYMS

AML	above mudline
ARA	Advanced Research Associates
BML	below mudline
BNC	bayonet needle connector
BOEM	Bureau of Ocean Energy Managment
BSEE	Bureau of Safety and Environmental Enforcement
C4	composition C-4 (explosive material)
CSA	CSA Ocean Sciences, Inc.
dB	decibels
DOI	U.S. Department of the Interior
EFD	energy flux density
ESA	Endangered Species Act
GOMR	Gulf of Mexico OCS Region
H6	composition H6 (explosive material)
Hz	Hertz
ITS	Incidental Take Statement
kHz	kilohertz
kPa	kilopascal
MAI	Marine Acoustics, Inc.
MOPU	mobile offshore production unit
MMPA	Marine Mammal Protection Act
MMS	Minerals Management Service
ms	millisecond
mV	millivolt
NMFS	National Marine Fisheries Service
NSWC	(U.S. Navy) Naval Surface Warfare Center
NTL	Notice to Lessees
OCS	Outer Continental Shelf
OCSLA	Outer Continental Shelf Lands Act
PETN	pentaerythritol
PROP	Platform Removal Observer Program
psi	pounds per square inch
PWAP	Pressure Wave and Acoustic Propagation
R	range (spreading loss)
RL	received level
s	second
SL	source level
SPL	sound pressure level
TAR	Technical Asessment Research Project
TL	transmission loss
TLP	tension leg platform
TNT	trinitrotolulene
TTS	temporary threshold shift
UWC	underwater calculator
UWCv1	underwater calculator version 1
UWCv2	underwater calculator version 2
V	volt
W	weight (of charge)
WD	West Delta OCS lease block area in Gulf of Mexico

1.0 INTRODUCTION

Oil and gas operations on the Federal Outer Continental Shelf (OCS) result in the placement of structures, equipment, and moorings into and onto the seafloor. The companies are obligated to decommission the offshore infrastructure when their activities are completed and remove the components from the OCS, as mandated under regulatory and lease requirements. Decommissioning is the process of ending the operations, removing the equipment and facilities, and returning the seafloor to its pre-lease condition. Under the OCS Lands Act (OCSLA), the U.S. Department of the Interior's Bureau of Ocean Energy Management (BOEM) establishes decommissioning obligations to which an operator must commit when they sign an offshore lease; these includes the requirement to apply for and obtain a permit for subsequent removal of wells and facilities. The U.S Department of the Interior's Bureau of Safety and Environmental Enforcement (BSEE) is responsible for regulating the decommissioning of OCS facilities in accordance with 30 CFR 250 Subpart Q. The regulations and lease agreements typically require the operator to remove all structures within one year of lease termination or before termination of the lease if either the operator or BSEE deems the structure unsafe, obsolete, or no longer useful for operations.

The OCSLA regulatory and lease requirements for decommissioning offshore platforms are designed to minimize the environmental and safety risks inherent in leaving unused structures in the ocean. Decommissioning an offshore platform generally entails plugging all wells supported by the platform, severing the well casings 15 feet below the mudline (BML), and removing the platform from its foundation by severing all bottom-founded components at least 15 ft BML. Additionally, the Bureau of Ocean Energy Management, Regulation and Enforcement (BOEMRE) published the Notice to Lessees and Operators (NTL) No. 2010-G05, "Decommissioning Guidance for Wells and Platforms," for lease holders in the Gulf of Mexico OCS Region (GOMR) to provide clarification and interpretation of Subpart Q requirements. The policy informs lease holders and operators of their responsibilities and provides definitions and timelines for decommissioning idle wells and associated platforms. Decommissioning idle wells and inactive platforms in a timely manner reduces potential environmental and navigational risks on the OCS.

Based on the most recent available data from BSEE (January 2016) (USDOI, BSEE, 2016), there are more than 2,325 existing structures the GOM OCS (**Figure 1** has locations as of December 2015). The four main types of structures found on the GOM OCS are multi-leg platforms (67%), caissons (23%), well protectors (8%), and floating facilities (2%), which includes spars, tension leg platforms (TLPs), and mobile offshore production units (MOPUs). The majority of structures are located off the coast of Louisiana in less than 300 ft of water.

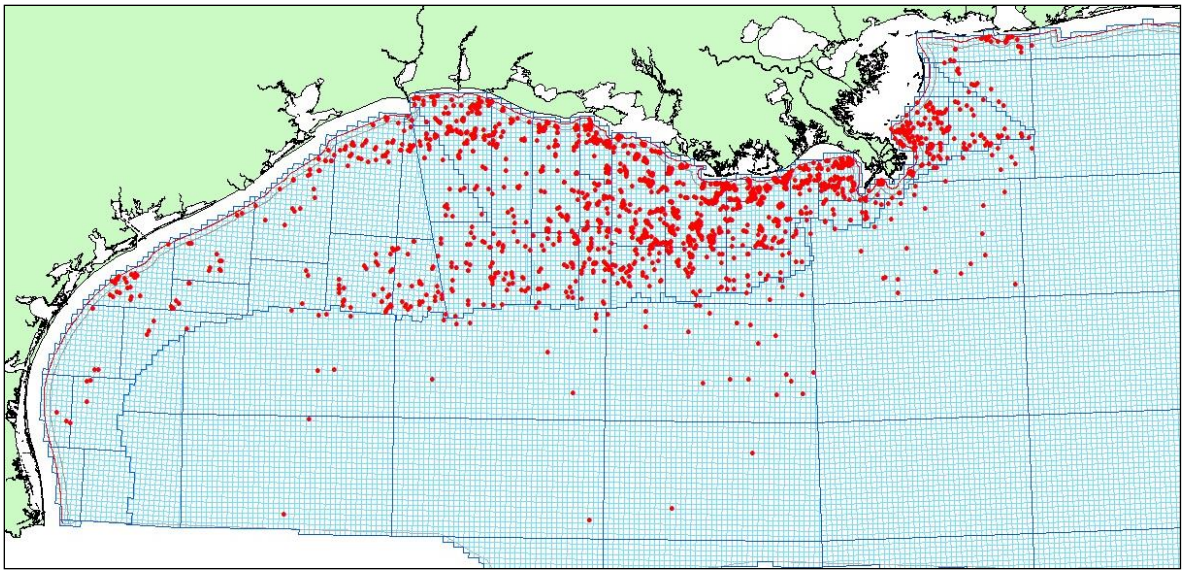

Figure 1. Structure locations on the Gulf of Mexico Outer Continental Shelf (as of December 2015).

As noted above, the most common type of offshore structure in GOMR is the conventionally piled platform (**Figure 2**). These structures are secured to the seafloor by steel pipes called piles (or pilings) driven through the legs of a tubular frame called a jacket. Only the upper portion of the jacket is visible above the water surface. Piles have varying diameters and wall thicknesses, and their number can vary from three to eight or more, depending on the platform's configuration and location on the OCS. The pile-to-jacket annulus in conventionally piled platforms is sometimes grouted. In most cases, several wells are drilled through long tubes, called conductors, placed through slots in the jacket. There can be as few as one or two wells or as many as sixty. The outermost pipe, called the drive pipe, may contain several inner conductors called casings.

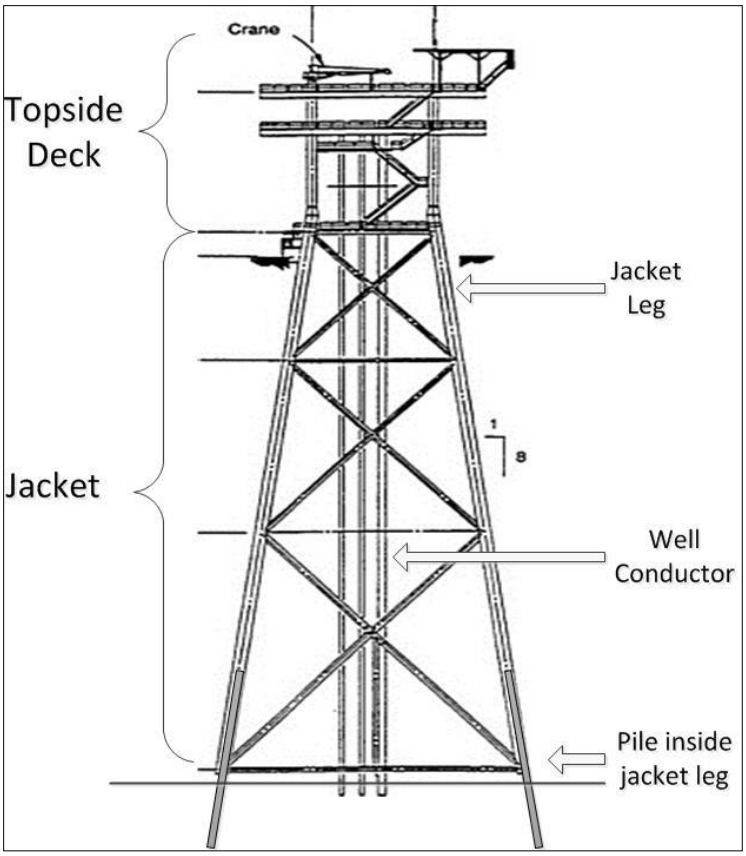

Figure 2. Typical platform or facility configuration found in the Gulf of Mexico OCS Region.

The methods used to sever bottom-founded components and other structural members will vary by facility, water depth, and other operational factors; however, BSEE categorizes the options as either mechanical or explosive severance. Currently, both severance methods are used equally.

Mechanical severance includes abrasive-water jets, sand-cutters, diamond-wire saws, carbide cutters, shears, and guillotine saws. This method generally proceeds more slowly than explosive severance options, because each target must be cut separately, and the logistics require additional personnel (often divers), or bulky support equipment is needed. Historically, the slower speed, additional personnel, and support spread result in more injuries and higher costs compared to explosive severance.

Explosive severance relies on the use of specially designed bulk or shaped charges. Charges are made up of explosive material with specific properties (i.e., velocity, density, brisance, specific energy, and weight strength) to produce enough stress, upon detonation, to completely sever the platform's bottom-founded components. The charge is generally deployed from above the water surface inside the pile or conductor and set at various depths to comply with the minimum 15-ft BML requirement and reshoots, if required. Current BSEE policy and the most recent Endangered Species Act (ESA) Biological Opinion allow operators to use charges with explosive weights up to 500 lbs; however, successful severance is typically made with smaller charges, from 50 to 200 lbs. Explosives allow multiple targets to be cut at once and typically require fewer technicians to deploy and detonate, which has historically resulted in fewer human injuries and lower costs compared to mechanical severance.

Though mechanical severance methods pose few environmental concerns, the use of underwater explosives has the potential to impact marine life, particularly, marine mammals, sea turtles, and fish, which can be harmed by explosive overpressures. Noise levels during these detonations may pose a

temporary acoustic disturbance to marine species. BSEE, as the permitting authority, and the operators who carry out the decommissionings, must do so in compliance with the ESA and the Marine Mammal Protection Act (MMPA). It is unlawful to "take" ESA-listed species; meaning it is unlawful to injure or harass a species listed as endangered or threatened under the ESA. BOEM and BSEE are subject to consultation requirements that may result in an Incidental Take Statement (ITS) and terms and conditions to be placed on decommissioning operations. In the GOMR, BSEE also coordinates with the National Marine Fisheries Service (NMFS) to petition for incidental-take rulemaking for marine mammals under the MMPA, which allows for subsequent Letters of Authorization (LoAs) to be issued to operators by NMFS for take coverage.

In the past, NMFS typically applied take-threshold criteria for explosives from models that were developed for the incidental-take authorization of U.S. Navy's shock trials. In these, large, open-water charges of 5,000 to 10,000 lbs are detonated within close proximity of new classes of warships to assess how well the ship can withstand damage and how well the crew can respond to mass system casualties (Department of the Navy, 1998, 2001). The conservative nature of these models resulted in high potential take estimates and large exclusions zones, on the order of 2 km or more, to be monitored during blasting operations. Conventionally, these conservative predictions of the impact zone have been used to satisfy MMPA and ESA requirements. However, explosive severance and, particularly, BML detonations are likely to produce lower pressure levels at the same propagation distances than open-water shock trial configurations, due to absorption, attenuation of energy by sediments, and the confinement of the explosion within well casings and platform piles. Conservative take estimates and large exclusion zones have been used for explosive severance because of a wide range of probabilistic error associated with insufficient in situ measurements from which to calculate the most plausible impact zone.

Previous explosive-severance studies conducted by the U.S. Department of the Interior's Minerals Management Service (MMS, now BOEM and BSEE) focused on determining the potential impact on the marine environment and increasing the accuracy of predicting pressure waves and acoustic levels radiating from blast events. By collecting acoustic data under various settings (i.e., varying cut depth, charge size), more accurate estimates of Pressure Wave and Acoustic Propagation (PWAP) can be calculated so that the agencies can apply appropriate mitigations to protect marine mammals and sea turtles, and also optimize operations (safety and efficiency) during detonations.

Before this study, MMS's Technology Assessment and Research (TAR) Project funded three similar, in situ PWAP projects working with various consultants and operators (**Figure 3**). The first, TAR Project No. 118, was overseen by the Department of the Navy's Naval Surface Warfare Center (NSWC). During the winter of 1988, it was carried out in coordination with MMS personnel and the Exxon Corporation, who measured 27 separate detonations at West Delta (WD) Block 30 (Connor, 1990). The Connor Study, as it is commonly called, included a set of developed, similitude equations, which were seen as the standard for calculating pressure ranges until NSWC questions the measurement. The second, TAR Project No. 429, was centered on developing improved linear shaped charge cutters; the project was modified during field testing to allow the deployment of an acoustic array to measure pressure wave characteristics (Saint-Arnaud et al., 2004). The severance/measurement activities were conducted in November 2003 at South Timbalier (ST) Block 21 structures. The third, TAR Project No. 570, was developed in 2006 to determine the effect of placement depth of the severance charges (15, 20, 25, and 30 ft BML) on the recorded PWAP (Poe et al., 2009). The in situ testing took place at two locations: in Eugene Island Block 128 during July and August 2007 and in East Cameron Block 32 in August 2008.

Figure 3. Approximate location of the current study in relation to previous Pressure Wave and Acoustic Properties (PWAP) measurement projects.

The current study was developed to be a successive project and applied a comparable methodology and equipment used in previous explosive severance studies to collect measurement data. The primary objective of this study, where possible, was to obtain additional in situ data points and charge parameters necessary to fill in information gaps from the previous projects. A secondary objective of this project was to provide supplemental data for validating and fine tuning previously-developed modeling used to establish impact zones for mitigative monitoring needed during decommissioning projects using explosives.

1.1 THEORETICAL BACKGROUND

A review of the theoretical background on shock wave attenuation and underwater propagation is provided in Section 2 of the TAR Project No. 570 report (Poe et al., 2009). A simplified explanation of the relevant concepts is offered here. The most basic form of the sonar equation can be used to outline the relevant issues (Eq 0).

$$RL = SL - TL$$

where RL is the received level, SL is the source level, and TL is the transmission loss. Source level is the amplitude of the explosion at a nominal range (typically 1 m). Transmission loss is the amount of amplitude decrease with range as the shock wave propagates outward. Subtracting TL from SL gives the received level at that particular range.

Safety ranges for marine protected species are set by NMFS at a conservative distance greater than that needed for the RL to meet the regulatory threshold (e.g., 23 pounds per square inch [psi]). The source level of an explosive charge in a free field is readily determined by its composition and weight. However, when a BML charge is encased in a pile, the sediment and the pile will absorb some of the energy produced by the explosion. The effective source level is reduced and was verified in previous studies (Poe et al., 2009, Connor 1990; Continental Shelf Associates, Inc., 2004; Saint-Arnaud et al., 2004; Kaiser et al., in prep; Frankel and Ellison, 2004; Dzwilewski and Fenton, 2003; Dzwilewski, 2014).

Once the shock wave enters the water column, its amplitude will attenuate with range (R). This is known as spreading loss or the decay rate. In a free field, the pressures of acoustic waves decay at a

rate of R^{-1} (decay rate of spherical spreading). The theoretical spreading loss for an open-water explosion is $R^{-1.13}$ (Arons et al., 1950), or slightly higher than spherical spreading. These decay rates are shown in **Figure 4** with both axes in logarithmic form. In this representation, the slope of the line can be used to measure the value of the exponent.

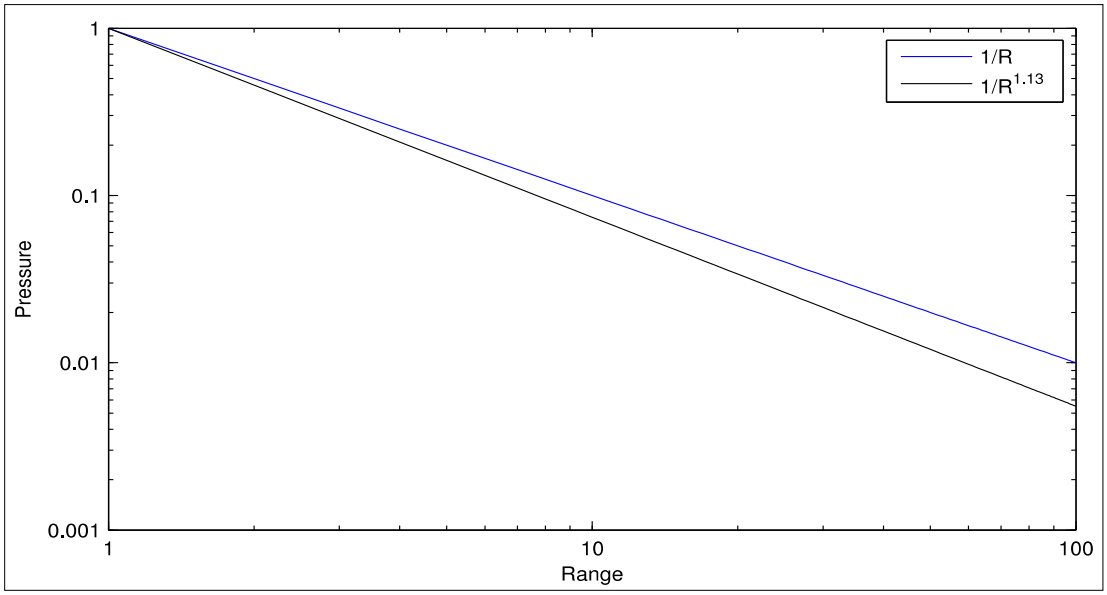

Figure 4. Theoretical decay rates or transmission loss rates.

In pure spherical spreading, the pressure drops as the reciprocal of R. The theoretical decay rate for explosions is $R^{-1.13}$. The slope of the pure spherical spreading line is -1 and the slope of the theoretical explosion line is -1.13.

1.2 BACKGROUND OF THE UNDERWATER CALCULATOR

In 2002, Applied Research Associates, Inc. (ARA) was contracted by MMS to develop a method to determine the shock wave propagation in the water column due to the underwater detonation of an explosive-severance charge. The research goal was to assess the impact that the detonations would have on marine life by developing a model that accurately estimates the shock effects caused by the detonation of a BML explosive charge inside a pile, leg, conduit, or other structural element of an oil and gas platform. The resulting model based on this methodology is referred to as the Underwater Calculator (UWC). The UWC is a spreadsheet-based tool that calculates the underwater shock, specifically the peak pressure, impulse, and energy flux density expected to result from the explosive detonation charges during explosive severance work. The tool is used to calculate the range from the explosive to a specified peak shock pressure and energy level that may result in impacts to marine life.

Version 1 of the UWC (UWCv1), published by ARA in 2003 (Dzwilewski and Fenton, 2003), calculated the propagation of acoustic energy from the explosive severance as a function of the pile diameter, pile wall thickness, and weight of the explosive used (25, 50, and 100 lbs). Numerical simulations using a representative distance of 30 m and 25-millisecond (ms) model run duration were performed to determine the amount of energy that is coupled to the water. The 30-m distance was chosen to be more than twice (2.3 times) the extent of the strong shock or nonlinear region as cited in Richardson et al. (1995). Each calculation was run out to a simulation time of 20 to 25 ms, which is the time it takes for a shock wave to propagate 30 to 37 m through water.

The simulations showed that less energy (30% to 70% reduction) is transferred to the water when the severance charge is confined than when detonated in open water. The inertial properties and structural strength of the pile and substrate must be overcome by the explosive charge before excess energy coupling into the surrounding water. The pile confinement has a greater effect than the substrate on the loss of energy coupling to the water because of the greater strength and density of the pile material. Some energy (typically less than 5%) is lost due to pressure wave propagation through the water trapped inside the pile. This minimal amount of energy propagates up through the pile opening and into the air (Dzwilewski and Fenton, 2003). The least amount of energy transmission into the water occurs when the explosive is placed BML within a pile, because this augments the effect of both the pile and the substrate on energy transmission.

MMS (now BOEM and BSEE) used the UWCv1 to calculate impact zones critical to protected species and for mitigation planning for the 2005 Programmatic Environmental Assessment (US DOI MMS, 2005). That information and the in situ comparisons done during TAR 429 (Saint-Arnaud et.al, 2004) were also used in the 2005 MMPA take authorization (Federal Register, 2008). When the UWCv1 was released, the MMPA take criterion was defined as a peak pressure greater than 12 psi for an explosive source. The NMFS has since revised this criterion and determined that temporary threshold shift (TTS) may occur at peak pressure levels greater than 23 psi (Federal Register, 2014).

To operate UWCv1, the user inputs a geometric profile that consists of explosive depth, slant range, and receiver depth; and physical properties, including pile diameter, pile wall thickness, explosive weight, and explosive type. The model offers several options in the type of explosives used: trinitrotolulene (TNT), composition H6 (H6), Pentaerythritol tetranitrate (PETN), composition C-4 (C4), or a user-defined explosive.

For the forward calculation, the outputs provided by the model are peak pressure, impulse (see Equation 1 in Dzwilewski and Fenton, 2003), energy flux density (see Equation 2 in Dzwilewski and Fenton, 2003), and explosive time constant at the specified point in the water column. The backward (or inverse) calculation provides the slant range for a specified energy flux density (EFD), decibel (dB) value, or pressure input.

UWC Version 2 (UWCv2), an updated version of the UWCv1, released by Dzwilewski (2014), accounts for the abovementioned newer take criterion of peak pressure levels greater than 23 psi and uses models of peak value as a function of range that have been refined and verified based on in situ data. These in situ data were collected as part of TAR Project No. 570 (Poe et al., 2009) and data collected by Connor (1990) during TAR Project No. 118. The models relating to TAR Projects No. 118 and No. 570 were developed by determining the best curve fit to each data set.

The TAR Project No. 570 data were collected for charges set at 15, 20, 25, and 30 ft BML during 20 internal (pile) severance detonations, with charges ranging from 25 to 145 lbs, and two open-water detonations using 5-lb charge weights. The conclusions drawn from the data indicate that increasing the depth BML of the explosive charge increased the attenuation of the pressure wave/acoustic energy and resulted in a size reduction of the marine protected species impact zones. Similarly, the TAR Project No. 118 (Connor, 1990) data were collected for main pile charges severed BML at depths of 8, 16, and 26 ft. Jacket leg and skirt piles were severed, along with well conductors. Charge weights of 25, 38, and 50 lbs were used. The data showed that, at 400 ft from the platform, the shock parameters were less than 10% of the values expected from an open-water detonation at the same range and same explosive weight.

A primary objective of this study was to obtain in situ data from decommissions of structures and charge parameters necessary to fill in any data gaps from the previous studies. To collect acoustic measurement data, this explosive severance study applied comparable methodologies and equipment as used in the previous studies. The project goal was to provide supplemental data for the validation and fine-tuning of the models used to develop the UWC. These new data yield information about the accuracy and robustness of the UWC Versions 1 and 2.

2.0 METHODS

2.1. TARGET SELECTION

Platform targets were selected based on consultation with BSEE and platform owner and operators to identify platforms that would be the best to use for model verification while still conforming to their decommissioning schedule. Each well and pile has specific physical properties that can influence the sound propagation. For well conductor severance, the charge is confined by the outermost drive pipe (caisson), the conductor pipe, and, in some cases, an inner casing pipe (**Figure 5**). For pile severance, the charge is confined by an outer jacket leg and an inner pile. The jacket leg and pile assembly are considered as one structure for the input parameters of diameter and wall thickness. The goal was to choose targets that would allow numerous detonations and charge configurations, such that the data collected would maximize charge types and BML configurations identified as high priority data gaps for refining the UWC. Targets were prioritized to increase the number and type of detonation (shot) measurements as inputs to the UWC, strengthening the UWC's value for potential use in estimating peak pressure and protected species safety zones during decommissioning activities that use explosive severance.

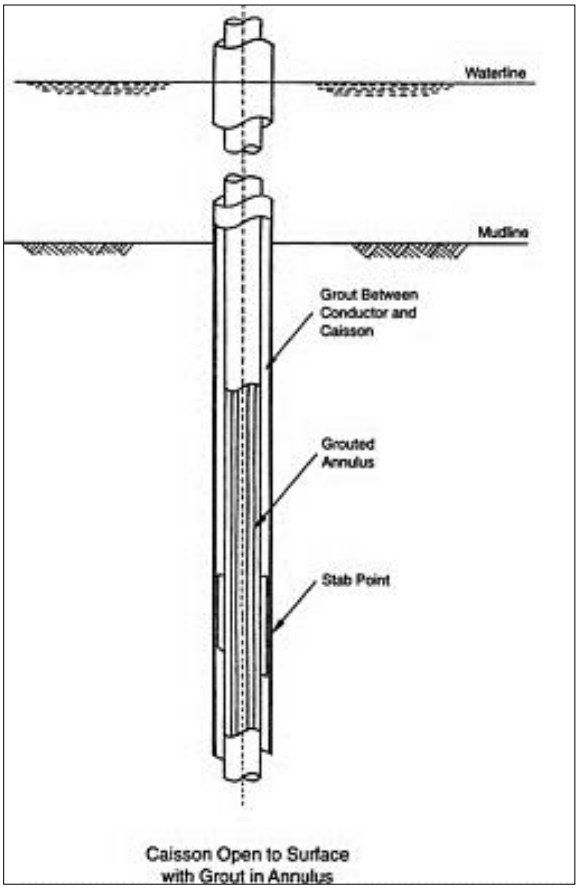

Figure 5. Cutaway of well conductor components.

Potential structures for removal were identified that offered an opportunity for at least 7 to10 detonation events with minimal mobilizations. Specifically, the availability of both well conductor and pile detonations, at least 15 ft BML, and requiring 100 lbs or more of explosives. Two appropriate platforms were selected: West Delta Block 40, platforms A and B (WD40A and WD40B). The

platform WD40A was located in the West Delta Block of the Gulf of Mexico at 29.04084020N/89.47700600W. The target consisted of eight well conductors and six piles located in 92 ft of water. Each conductor was 24 to 28 inches in diameter and had a wall thickness of 0.5 inches. Each pile was 36 inches in diameter, with a wall thickness of 1.75 inches.

The platform WD40B was also located in the West Delta Block of the Gulf at 29.04090000N/89.48190000W. The target consisted of five piles located in 92 ft of water. The piles were 36 inches in diameter with a wall thickness of 2.25 inches.

2.2 FIELD DETONATION DESIGN

Explosive charges made of composition B explosives were used to sever the piles and well conductors of WD40A and WD40B. During the preparation of these structures for removal, welders cut deck with associated topsides (equipment and helicopter pad) from the jacket approximately 12 ft above the waterline and transferred the assembly to a material barge using the main crane on the derrick barge. Deck removal deck allowed access to high pressure jet cleaning of the internal well conductors and piles to the specified severance cut depth. The specific structures removed during this test were permitted by BSEE for 200-lb explosive charges detonated at 15 ft BML. The explosive severance charges were lowered by crane to the predetermined depth BML and secured. The charges were then primed (delay detonator attached), and the derrick barge was moved to a safe location (at least 500 ft away) from the platform jacket. NMFS observers from the Platform Removal Observer Program (PROP) then performed an aerial observation by helicopter for 45 minutes. Aerial observation patterns make a clockwise spiral from the platform out to the edge of the impact zone (NOAA, 2006); or 3,086 ft for this removal scenario. Halfway through the survey, the observation aircraft periodically diverges from the spiral pattern to scan outside the perimeter of the impact radius to confirm that no animals are approaching the impact zone. The NMFS observers completed the required observation period and confirmed that the observed area around the platform was clear of marine mammal and sea turtle species immediately before detonation.

Upon NMFS clearance confirmation, the explosives were detonated using a minimum 1-s delay detonator between each charge. The derrick barge was then moved back into position (next to the platform) for rigging and lifting the severed conductor wells and platform jacket (**Figure 6**). The conductor wells were pulled out of the slots first and then the entire jacket structure was removed from the seabed. The decommissioned platform jackets and conductor wells were fastened to a materials barge and transported to an onshore disposal facility.

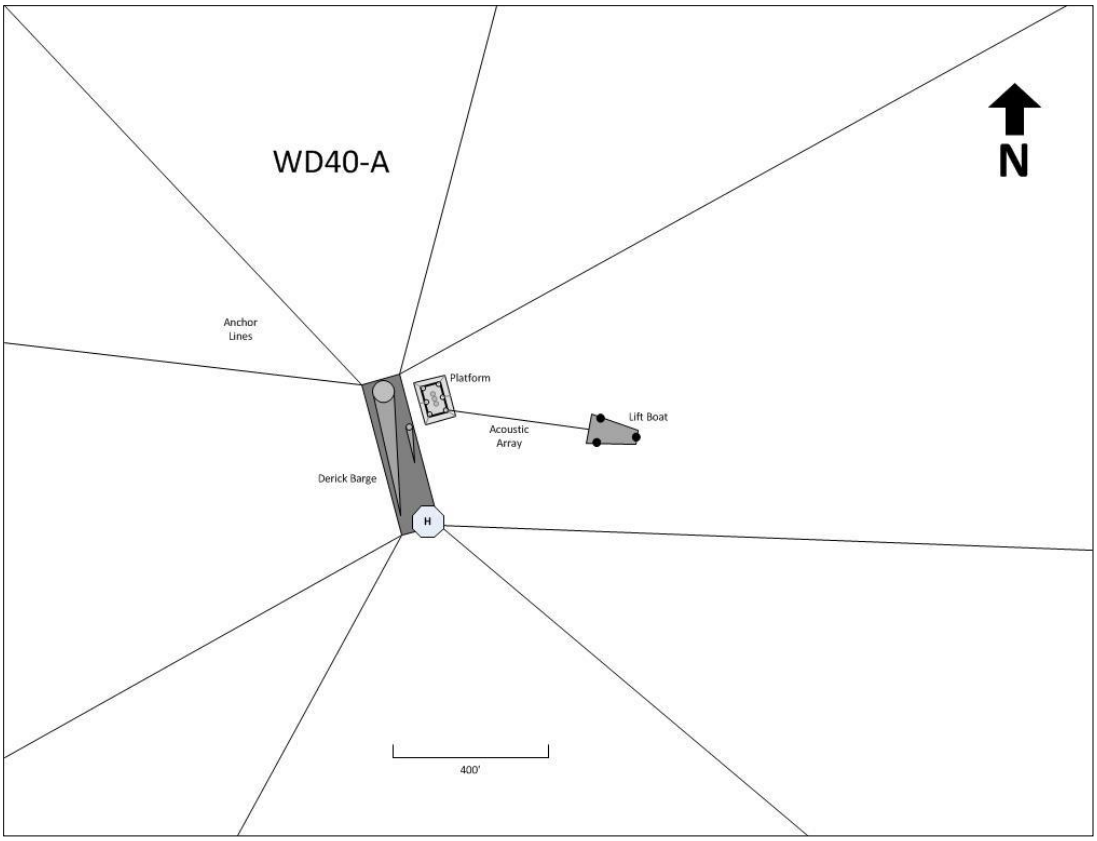

Figure 6. Top-down view of the project equipment arrangement showing the derrick barge with anchor lines, lift boat (recording platform), and platform.

This placement was similar for both removal sites WD40A and WD40B.

2.2.1 Well and pile sever information

A total of eight well conductors at the WD40A platform were severed at 13:01 hours on 24 October 2014 (**Table 1** and **Figure 7**). There was a 1-s delay between each shot.

Table 1. WD40A well conductor shot parameters.

Shot	Target Name	Charge Weight (lb)	Charge Depth BML (ft)	Outer Drive Pipe Diameter (in.)	Conductor Diameter (in.)	Casing Diameter (in.)	Wall Thickness (in.)
1	Well A-11	75	25	24	9.625	n/a	0.5
2	Well A-4	100	25	24	10.75	7.625	0.5
3	Well A-9	100	25	24	10.75	7.625	0.5
4	Well A-2	100	25	24	13.375	10.75	0.5
5	Well A-7	100	25	24	16	10.75/7.625	0.5
6	Well A-8	75	15	24	10.75	n/a	0.5
7	Well A-1	100	15	28	9.625	n/a	0.5
8	Well A-3	75	15	24	10.75	n/a	0.5

BML = below mud line; n/a = not applicable.

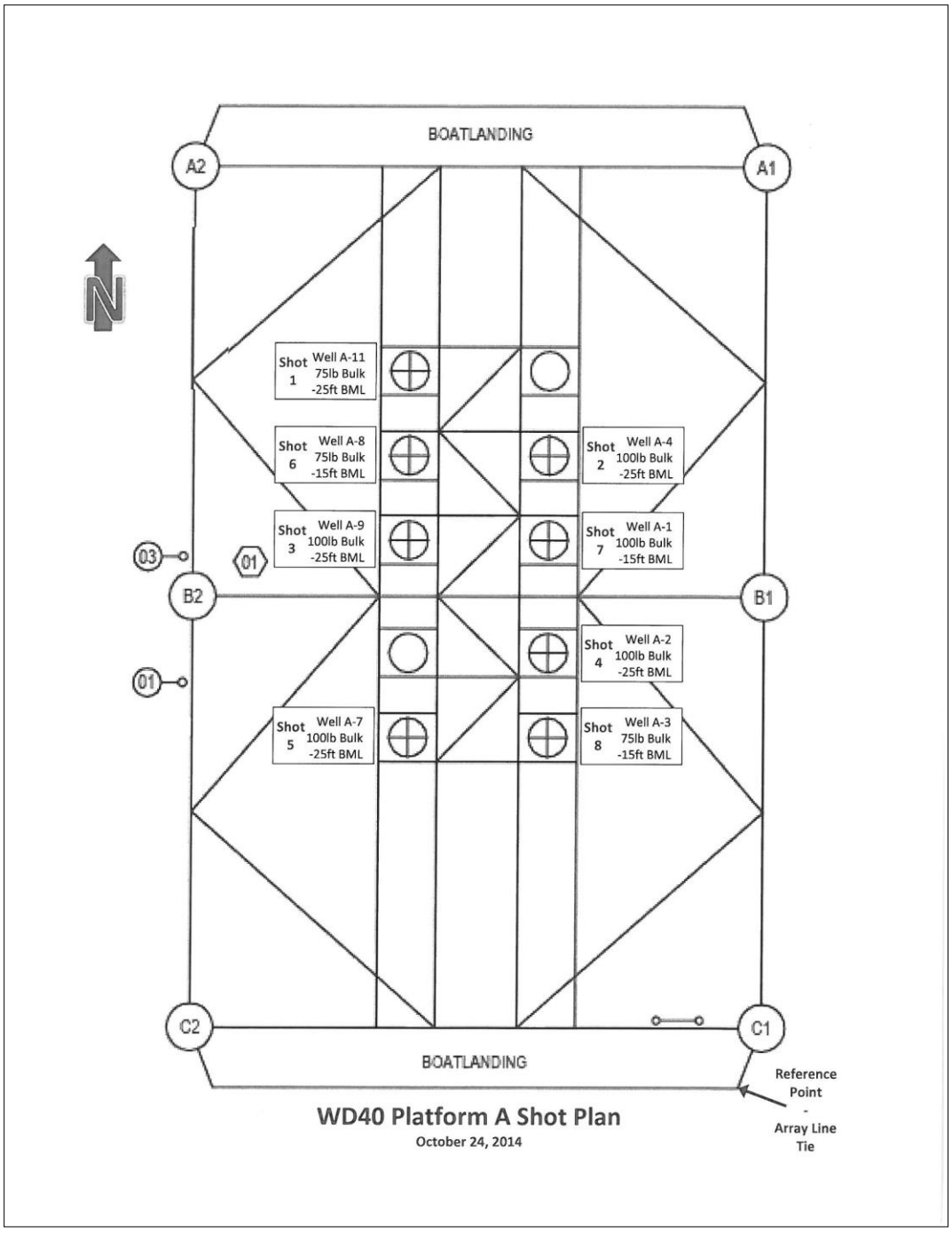

Figure 7. Top-down perspective of the shot plan at WD40A well conductors.

A1 and C2 are the platform support legs; the arrow points to the location of the acoustic sensor array attachment, the reference point is the location of the pre-detonation calibration charge.

The six piles at platform WD40A were severed at 11:36 hours on 25 October 2014. The following list describes each pile and the order of detonation (**Table 2** and **Figure 8**). There was a 2-s delay between each shot.

Table 2. WD40A pile shot parameters at 11:36 hours on 25 October 2014.

Shot	Target Name	Charge Weight (lb)	Charge depth BML (ft)	Diameter (in.)	Wall Thickness (in.)
1	A2	200	20	36	1.75
2	A1	200	20	36	1.75
3	B1	200	20	36	1.75
4	C1	200	20	36	1.75
5	C2	200	20	36	1.75
6	B2	200	20	36	1.75

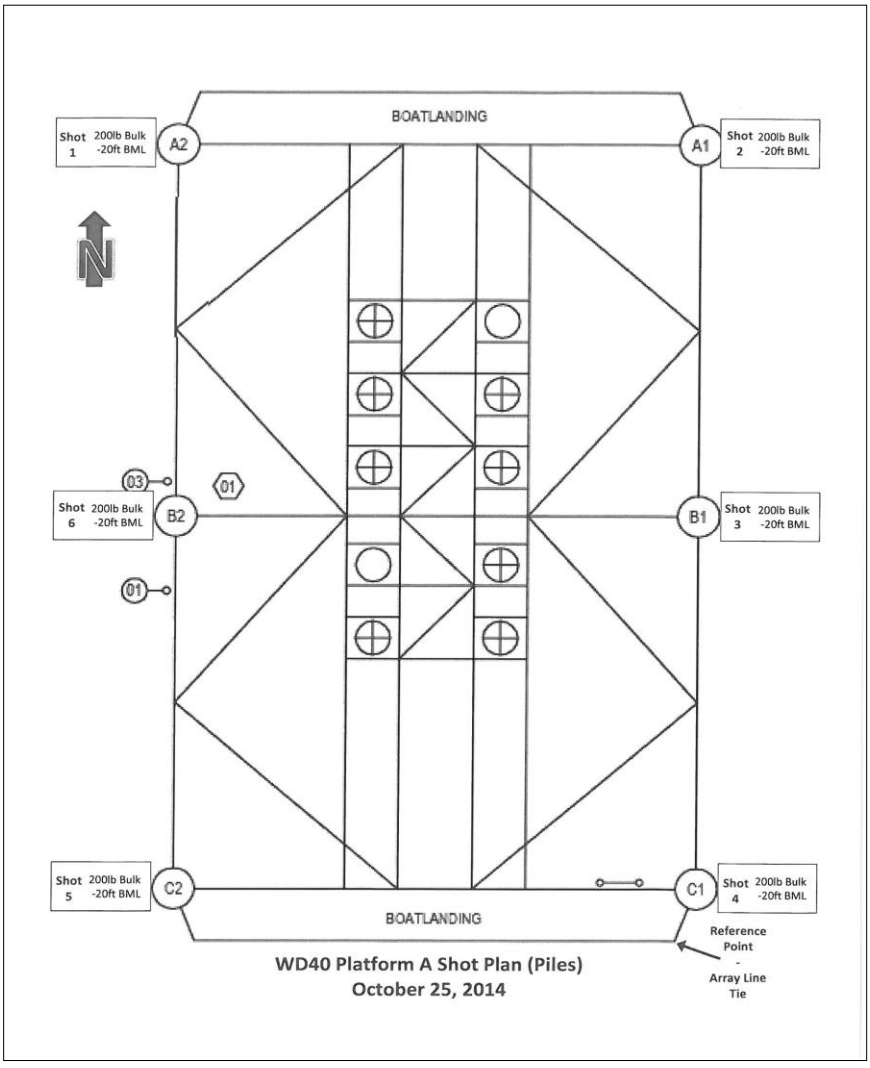

Figure 8. Top-down perspective of the shot plan schematic for WD40A piles (A1 and C2).

The arrow points to the location of the acoustic sensor array attachment, the reference point is the location of the pre-detonation calibration charge.

Five piles of the WD40B platform were severed on 28 October 2014 (**Table 3**) at 15:11 with a 2-s delay between shots. Pile A2 was not severed due to problems encountered while jetting (cleaning) piles for charge placement.

Table 1. WD40B pile shot parameters.

Shot	Target Name	Charge Weight (lb)	Charge depth BML (ft)	Pile Diameter (in.)	Wall Thickness (pile and jacket leg) (in.)
1	A1	200	20	36	2.25
2	B1	200	20	36	2.25
3	C1	200	20	36	2.25
4	C2	200	20	36	2.25
5	B2	200	20	36	2.25

2.3 FIELD DATA COLLECTION

2.3.1 Acoustic Array

The sensor array used to collect these data was based on the successful designs used in the previous TAR Projects No. 429 and No. 570 (Saint-Arnaud et al., 2004; Poe et al., 2009). CSA and Marine Acoustics, Inc. (MAI) constructed a transducer array consisting of 12 PCB Piezotronics, Inc. (PCB) W138A02 Tourmaline ICP® underwater blast sensors. These sensors have a measurement range of 1,000 psi (6,895 kilopascals [kPa]), sensitivity at (±15%) 5 millivolt (mV) psi^{-1} (0.73 mV kPa^{-1}), a low-frequency response of (-5%) 2.5 Hertz (Hz), and resonant frequency of ≥ 1,000 kilohertz (kHz).

Sensors included measured-to-length marine waterproof cabling that terminated with a bayonet needle connector (BNC) installed by the manufacturer. The 12 individual sensors were powered by three four-channel PCB 482C05 charge amplifiers. A Yokogawa DL850 data acquisition and analysis system was used to process, display, and record data. This Yokogawa was equipped with six, 2-channel 1 MS s^{-1}, 16-bit, high-speed modules (model number 701251) that were used to provide analog to digital conversion with sufficient dynamic range and temporal resolution.

To capture the desired data for each blast configuration, three near-field acoustic arrays were deployed that consisted of three transducers each and three far-field acoustic arrays were deployed that consisted of one transducer each that were located at predetermined depths (proportional to the water depth and platform structure). The array of sensors is diagrammed in **Figure 9**.

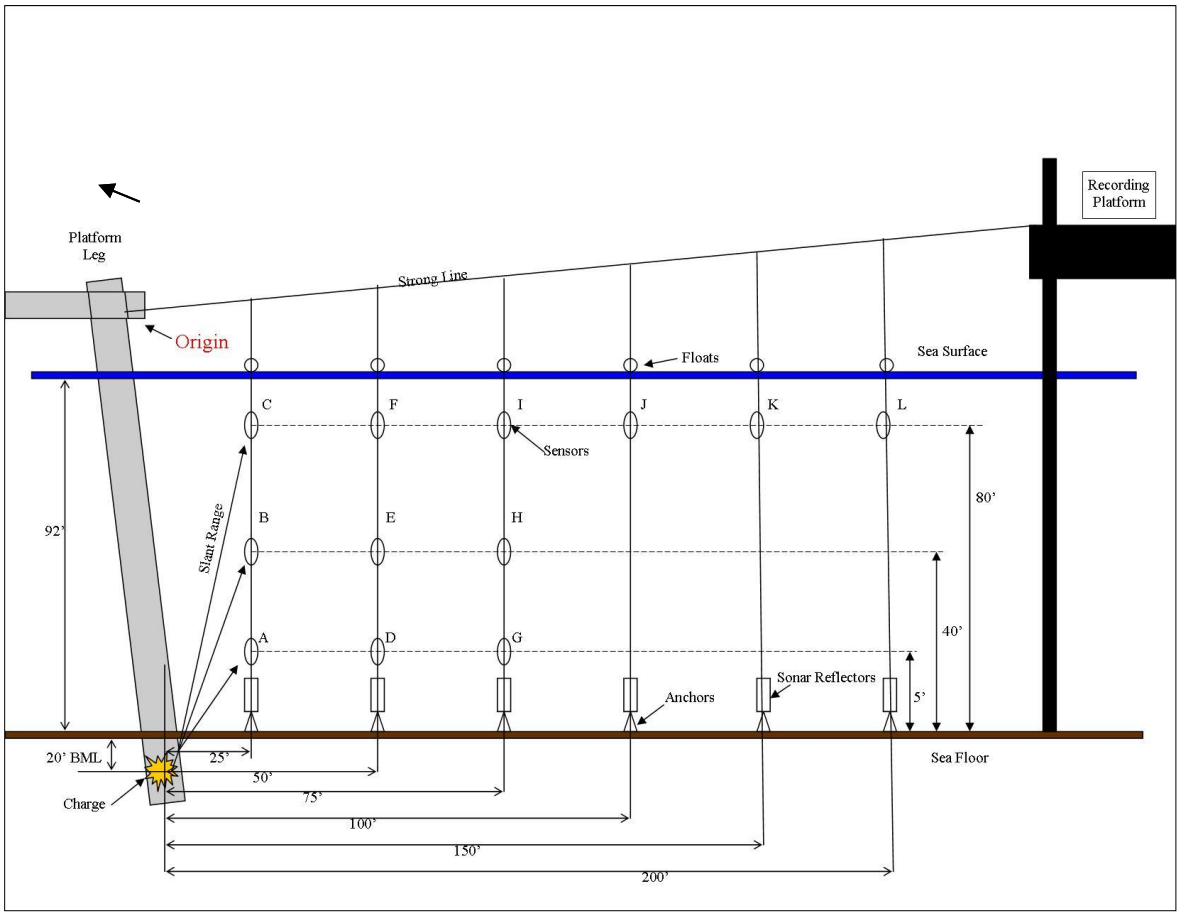

Figure 9. Schematic drawing of array configuration.

Sensor cables are not shown here; however, a single cable ran from each sensor to the electronics on the lift boat. The location of the reference origin of the array is indicated by an arrow and "origin" in red.

The array methodology and deployment configuration was similar to the methodology used during TAR Project No. 570 (Poe et al., 2009). The vertical arrays were deployed from a small watercraft launched from the lift boat. Each array was attached to a 4-mm braided plasma line equipped with a sonar reflector and anchor. Once the lift boat was positioned, a small workboat (approximately 15 ft) was used to attach the coated steel cable (strong line) to the designated pile of the target platform. The strong line was stretched taut from the target structure to the lift boat that provided housing for the recording equipment. The strong line had floats placed at the locations where each downline or anchor line was placed. Each downline assembly consisted of an anchor, a sonar reflector, the vertical non-stretch plasma line, and appropriate number of cabled sensors (**Figure 9)**. The downline assembly was installed by lowering the anchor to the bottom, then attaching the plasma line to the horizontal strong line. The sensor cables were routed along the strong line, and the cable connectors were attached to the data acquisition equipment on the lift boat. This procedure was repeated for each downline assembly and sensor cable.

Once the workboat was retrieved, BSEE personnel deployed the Mesotech MS 1000 sector scanning sonar to record the positions of the sonar reflectors located at the bottom of each downline. The sonar data, combined with the known positions of the surface floats, were later used to calculate the three-dimensional (3D) coordinates of each sensor.

Near the bow rail of the lift boat (recording location) was an 8 ft x 10 ft steel container, which was used as a weatherproof equipment lab. The Yokogawa and signal conditioners were located in this lab as well as storage for supplies and backup equipment. The cables with BNC connectors from each sensor were run over the bow and into the lab. Power for the equipment was provided by a combination of a small generator, 12-V batteries, and ship power.

Before each decommissioning event, the charge weights were input into UWCv2, using the open-water setting, to predict the amplitude of the signal at each sensor. These predictions determined the appropriate sensitivity setting for each data channel of the Yokogawa recorder for each explosive severance event to ensure that the incoming data signals did not exceed the voltage range of the recorder, a condition known as "clipping".

Before each detonation, the derrick barge backed away from the target platform, and the lift boat was raised several feet above the sea surface for safety and to protect the ship systems from the blast. Raising the lift boat pulled the strong line taut and therefore provided and maintained accurate spacing in the downlines. A small calibration charge consisting of 2 ft of detonation cord was used to verify that the sensor and data recording equipment were working properly before each decommissioning event. This ensured that data collection equipment was functioning properly before the explosive charges were detonated.

Before each explosive severance event, the field acoustician and BSEE personnel coordinated the protocol and timing between charges with the explosives director. When all preparations were finalized, the explosives director gave a two-minute detonation warning notice over the radio. The Yokogawa recorder data acquisition process was started at least 30 s before the detonation event. Explosive charges were spaced 1 s apart for the well conductor severance event at WD40A and 2 s apart for the pile severance events to allow reverberation to attenuate before the next explosive charge detonated.

2.4 DATA MEASUREMENT

The Yokogawa recorder was stopped shortly after detonation. The acquired data were transferred via secure digital card to a Dell Dimension workstation, where they were converted from the proprietary Yokogawa format (WDF) into a standard .wav audio file format using the Yokogawa supplied WDFcon utility.

The remaining analyses were conducted on a MacBook Pro using Matlab 2014a (Mathworks, 2014). The voltage data were loaded and converted into pressure values (psi) using the calibration values provided by PCB (**Table 4**). A sample recording is shown in **Figure 10**, where five discrete explosion signals can be seen clearly.

Table 2. Transducer calibration data.

Yokogawa Channel	Signal Name	Distance AML (ft)	Cable Length (ft)	PCB Tranducer	Serial Number	Sensitivity (mV/psi)
1	A	5	450	138A01	10132	5.007
2	B	45	425	138A01	10140	4.919
3	C	80	400	138A01	10139	5.034
4	D	5	400	138A01	10138	5.033
5	E	45	375	138A01	10137	5.284
6	F	80	350	138A01	10135	5.057
7	G	5	375	138A01	10136	4.704
8	H	45	350	138A01	10134	5.191
9	I	80	325	138A01	10144	5.009
10	J	80	300	138A01	10142	5.003
11	K	80	250	138A01	10143	4.880
12	L	80	200	138A01	10141	5.138

AML = above mudline; mV = millivolt; PCB = PCB Piezotronics, Inc.; psi = pounds per square inch.

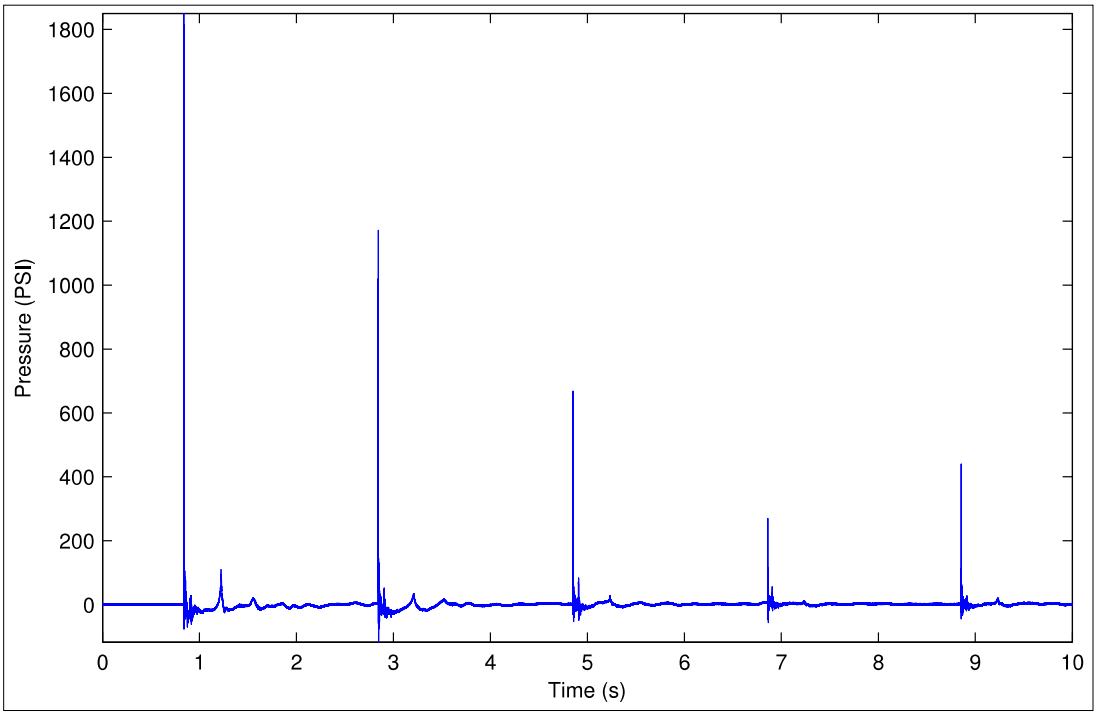

Figure 10. Sample data waveform showing five explosive events.

The following amplitude metrics were generated for each signal on each recording channel:

(1) Peak pressure (reported in psi and megaPascals)
(2) Impulse (reported in psi-seconds and kiloPascal-seconds)
(3) Energy flux density (EFD; reported in psi-inch and kiloPascal-meter)

Peak pressure is simply the maximum pressure value for each signal on each channel. Impulse (I) was calculated with Equation 1:

$$I(t) = \int_0^{\tau} P\,(t)dt \qquad (1)$$

where P is pressure and τ (tau) is the integration time of the impulsive signal. The integration time was set as five times the time constant (Swisdak, 1978). The time constant is defined as the time needed for the peak pressure (Pm) to decay to the defined value of Pm/e, where e = ~2.718. **Figure 11** illustrates the procedure to determine the time constant (redrawn from Swisdak, 1978). The solid line represents exponential decay. As per Swisdak (1978), exponential decay is expected to occur until about one time constant (θ). After that, the actual decay in pressure is expected to occur more slowly, shown as the dashed line.

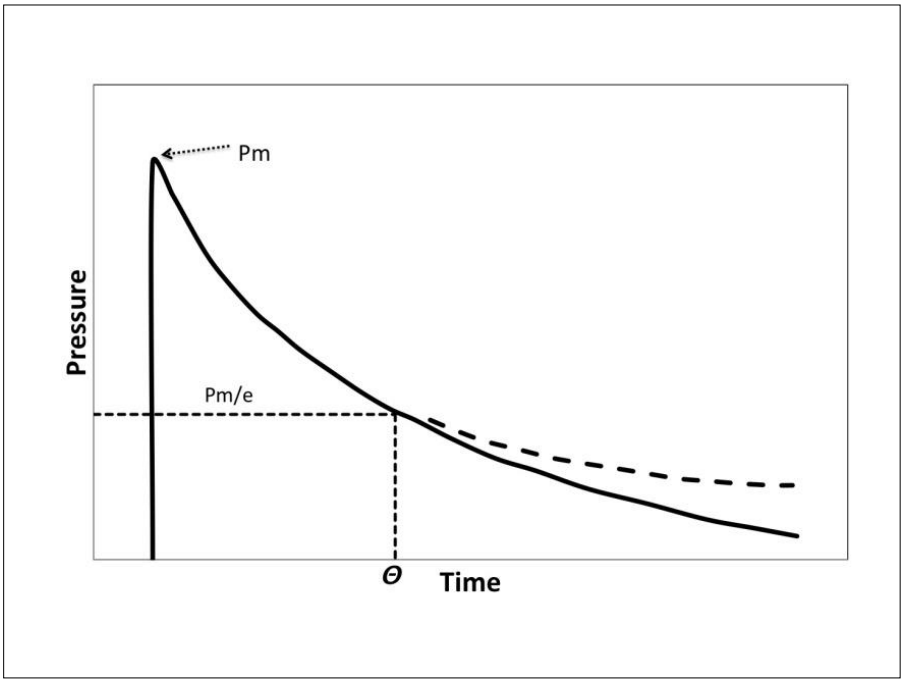

Figure 11. Determination of the time constant.

The EFD was calculated using Equation 2:

$$E_f(t) = \rho_0^{-1} c_0^{-1} \cdot \int_0^{\tau} p^2\,(t)dt \qquad (2)$$

The τ (tau) value derived for the impulse calculation was used in this calculation.

Moving from theory to measured data introduced complexities in the analysis of measurement results. The measured signals frequently had multiple peaks or otherwise did not conform to the theoretical decay pattern, complicating the determination of the value of theta. An exponential decay function was fit to the pressure time series (**Figure 12**). The time constant was taken as the time required for the fitted exponential decay function to reach the criterion value (Pm/e). If the recorded time-pressure series did not support the curve fit, the impulse measurement for that signal was discarded.

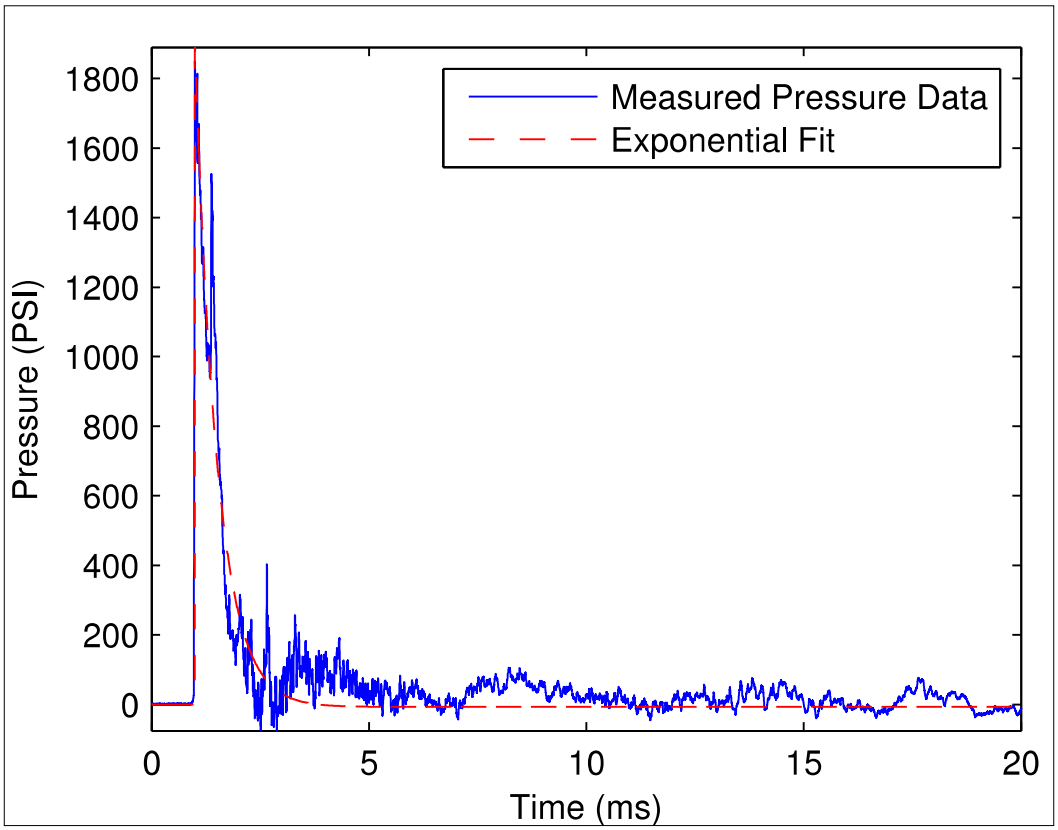

Figure 12. Exponential fit-to-measured data.

The blue line shows the measured pressure values, and the red line shows the exponential fit to the data.

2.5 SLANT RANGE CALCULATION

The precise manner of array deployment enabled an accurate estimation of the 3D positions of the sensors and the explosive charges. Thus, the distances between them in the X, Y, and Z planes were calculated, and the total slant range (**Figure 13**) from each charge to each sensor was determined. In addition to the positional data provided by the blueprints of each platform, the origin of the local coordinates for each platform was recorded at the attachment point of the strong line to the designated pile (seen in **Figure 9**). The dimensions of the platform and the BML depth were then used to determine the 3D locations of the charges.

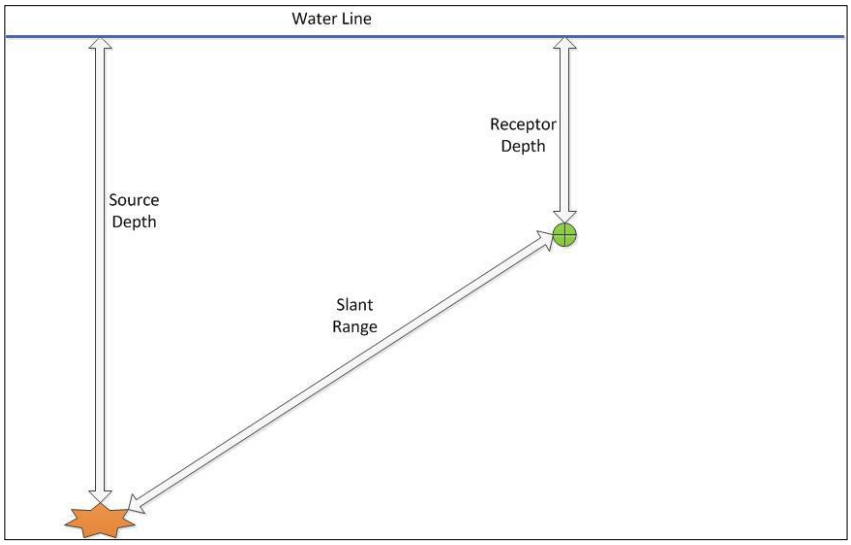

Figure 13. Slant range.

The Mesotech data were used to calculate the horizontal range and bearing of each sonar reflector from the position of the pile to which the strong line had been attached. The assumption was made that the surface float was directly above the sonar reflector. Thus, the platform geometry and Mesotech data provided the inputs for the X and Y planes. An example of this is shown in **Figure 4**. The distance in Z direction was the charge depth, added to the measured height of each sensor above the seafloor. The X, Y, and Z distances were used to calculate the slant range from each charge to each sensor.

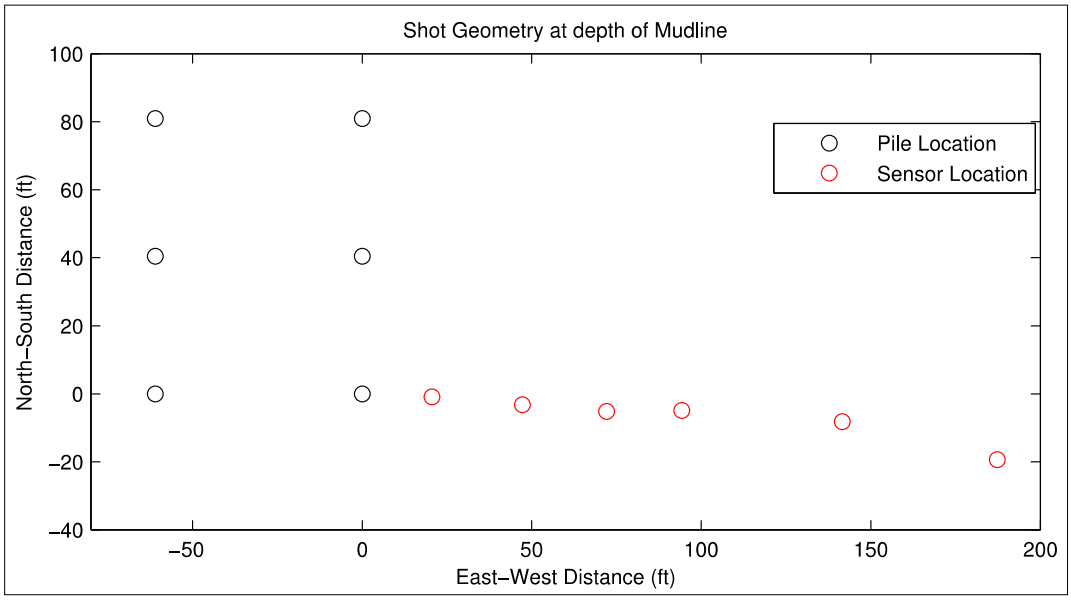

Figure 14. Example of the spatial relationship for the pile locations determined from the platform blueprints and the sonar reflectors determined from the Mesotech data.

3.0 RESULTS

Data are presented as both a function of slant range and the reduced range (Urick, 1983). The reduced range is the range divided by the cube root of the charge weight. In a free-field environment, the received level of peak pressure, from a charge of weight, W, is defined as:

$$\log_{10}(Peak\ Pressure) = Constant - 1.13 \log_{10}\left(R \cdot W^{-1/3}\right)$$

Plotting the peak pressure compared to the reduced range allowed simultaneous comparison of data from different explosions with varying charge. When plotted as a function of slant range, data from different size charges must be considered separately.

Field measurements were compared with various predictions produced by the UWCv1 and UWCv2. UWCv1 requires specification of pile parameters (diameter, thickness), whereas UWC v2 has a predetermined set of scenarios (e.g., main pile Connor or well conductor, TAR Project No. 570) that incorporate values for these variables. The UWCv2 predictions included those for a free-field explosion, the main pile, and the well conductor with the Connor and TAR Project No. 570 options. UWCv1 predictions were made using the exact values from each explosion.

3.1 MEASUREMENT RESULTS

Summaries of the results for each individual detonation event (WD40A well conductors, WD40A piles, and WD40B piles) using UWCv2 are provided in **Appendix 1**. A detailed list of sensor measurements for each shot is provided in the Appendix.

3.1.1 Measurement Results from WD40A Well Conductors

The first measurements were made on 24 October 2014 when the well conductors were explosively severed. **Figure 15** illustrates the geometry of the well conductor, piles, and locations of the pile charges for platform WD40A. Data were collected on 11 of 12 of the sensors. One of the sensor cables was accidently cut during deployment before the explosives were detonated. This cable was repaired and the sensor was returned to service the following day.

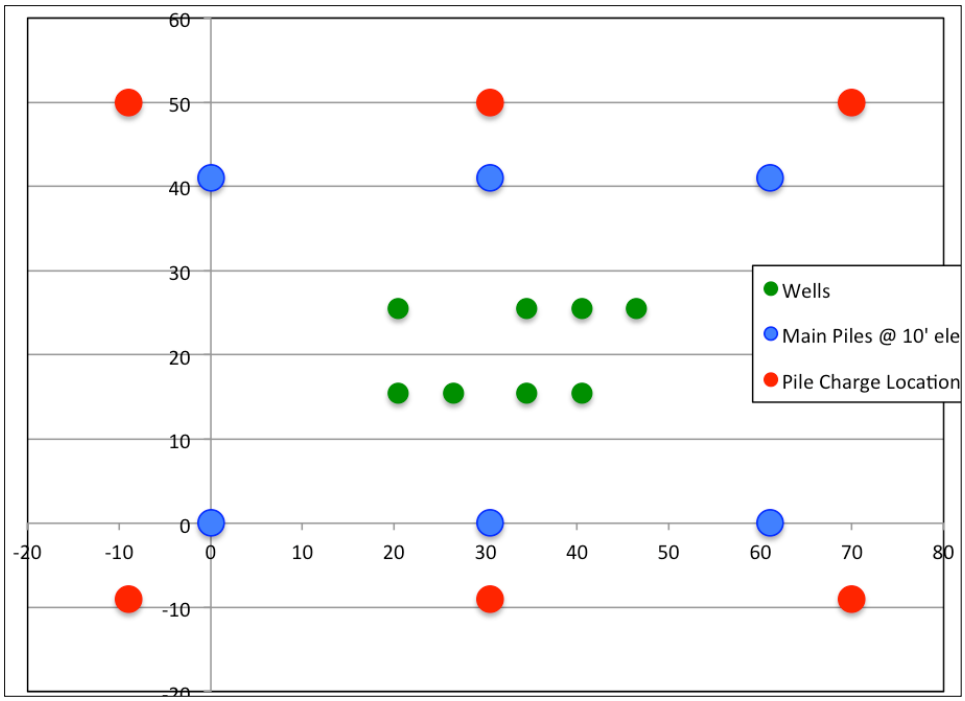

Figure 15. Topside plan view of the main piles and well conductors of the WD40A platform.

The main piles are slanted at a slope of 10%, so the positions of the piles at the surface and the positions of the charges BML are offset. The positions of the main piles are shown at the 10-ft elevation, as taken from the original plans (distances are in feet). The positions of the charges BML were determined from the slope of the main piles (10%).

The final charge locations and configurations that were used as input for the UWCs are shown in **Tables 1** through **3**. The pressure results for each detonation shot are shown in **Figure 16**.

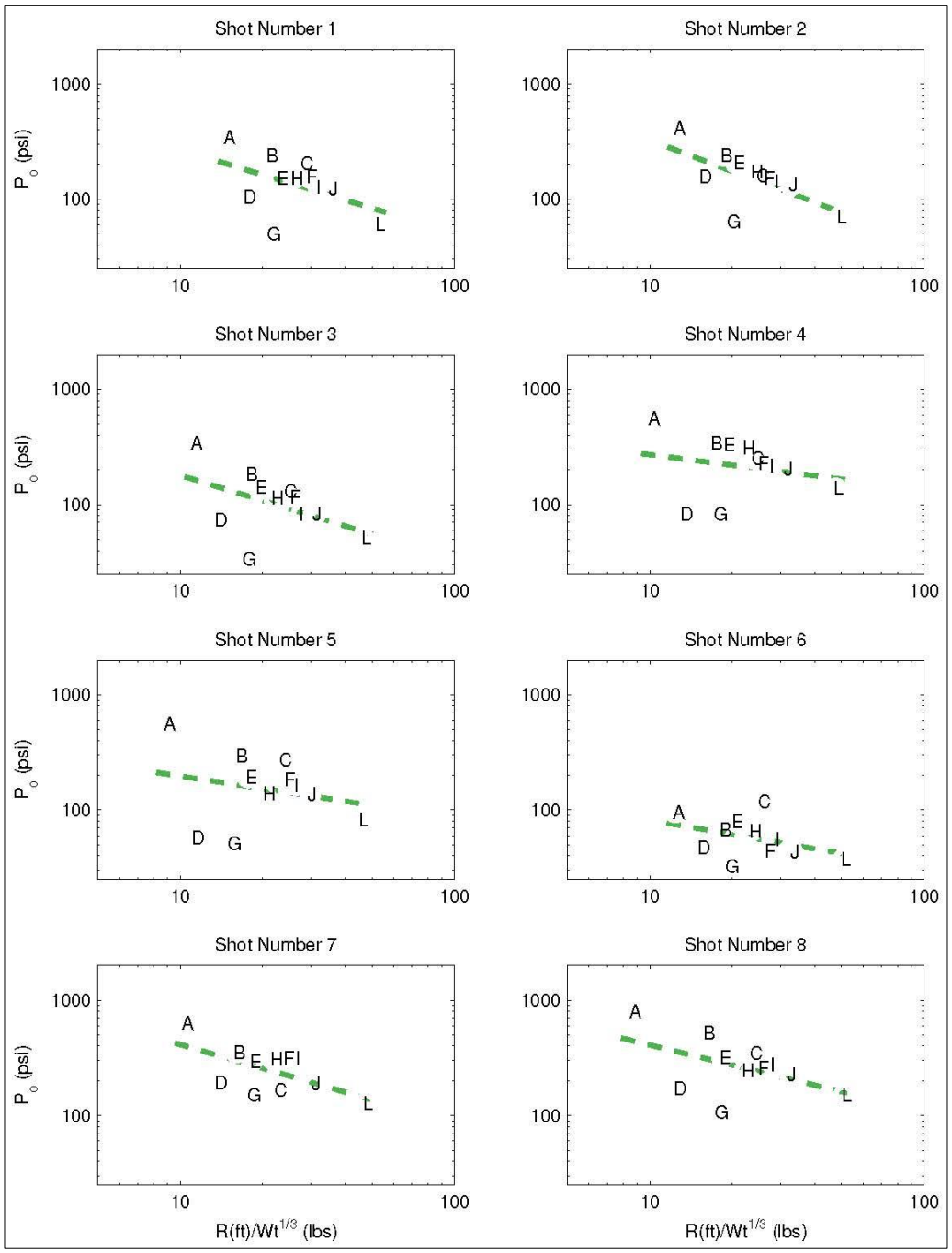

Figure 16. Peak pressure measured on each sensor (black letters) as a function of the reduced range for the WD40A well conductor shots.

A log-log fit of the data is shown as a green line.

The data in **Figure 17** show what appear to be two anomalous data points in each of the detonations shots (e.g., the two data points in the lower left corner for shot number 8). These anomalous points were recorded on the near-bottom sensors D and G. **Figure 16** shows the same data with these two sensors removed. The relationship between pressure and the reduced range axis is much more consistent. Potential reasons for the anomalous data points are discussed in **Section 4.0**.

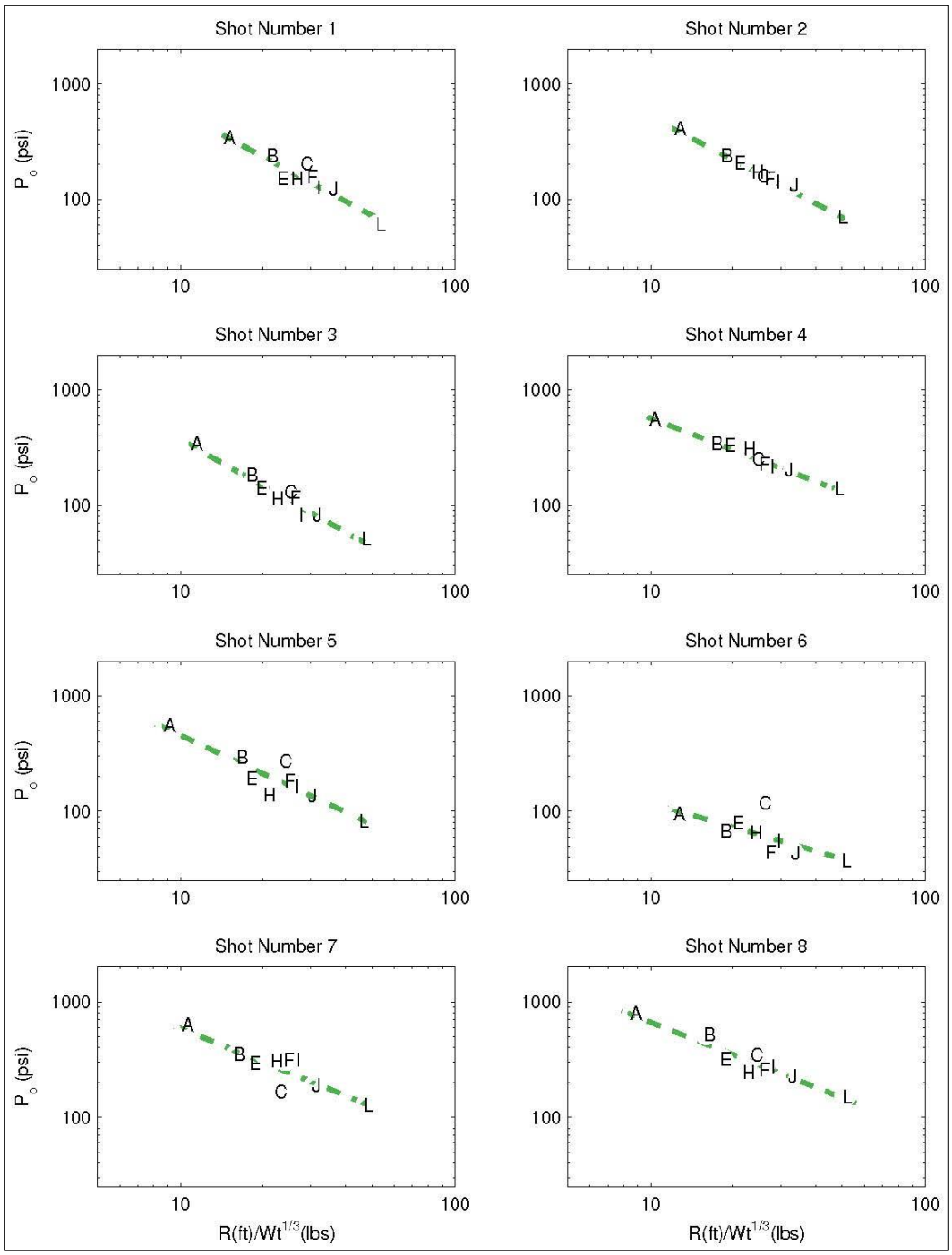

Figure 17. Peak pressure measured on each sensor (black letters) as a function of the reduced range axis for the WD40A well conductor shots. A log-log fit of the data is shown as a green line.

The data from the 75-lb charges (n = 3) from the WD40A well conductor detonations (open circles) were combined (**Figure 18)**. The predictions of the UWC (Versions 1 and 2) are plotted for comparison. The long red line in this (and the following) figure represents the linear curve fit to the measured data, which has a slope of -1.042. The UWC predictions and the curve-fits represent the decay function of the pressure amplitude with range. The 100-lb charge data from the 100-lb charges (n = 5) from the WD40A well conductor shots were also combined (**Figure 19**). The slope for the line fitted to those data is -1.121.

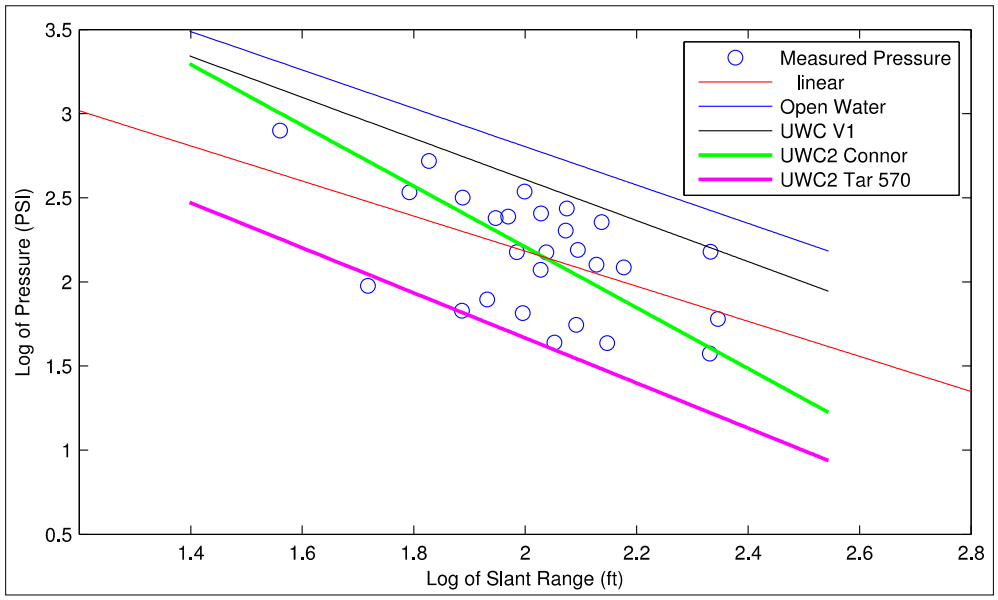

Figure 18. Pressure data for all 75-lb charges and linear curve fit for each UWC prediction (without sensors D and G). Slope (red line) is -1.042.

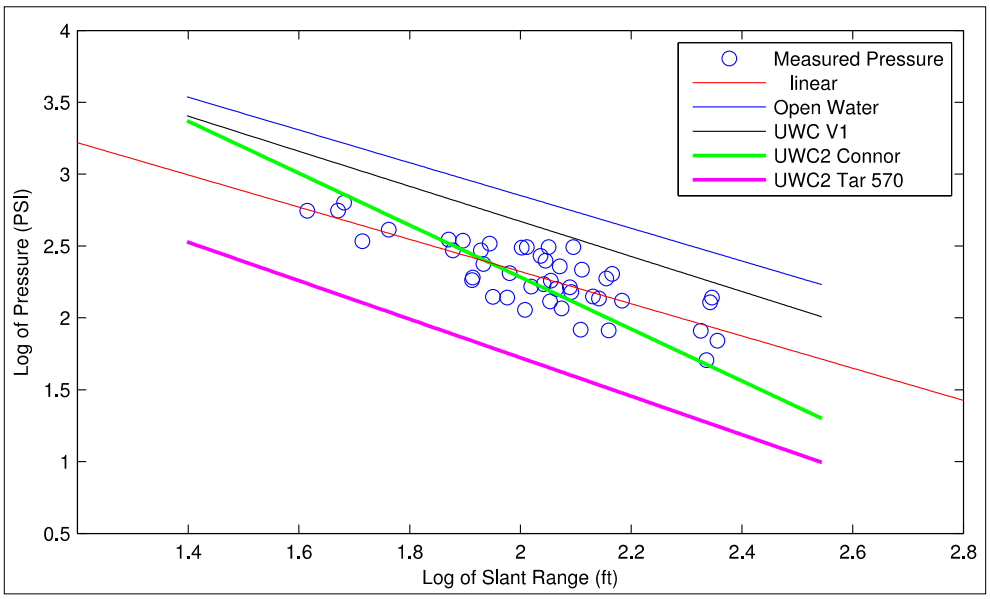

Figure 19 Pressure data for all the 100-lb charges (without sensors D and G). Slope (red line) is -1.121.

Both **Figures 18** and **19** show that the 75- and 100-lb data (red line) have respective decay rates of $R^{-1.04}$ and $R^{-1.21}$, which are similar to those of the open water, the UWCv1 (gray line), and the UWCv2 TAR 570 (pink line) predictions ($R^{-1.13}$). The amplitude of the measured data is intermediate between the two predictions.

3.1.2 Measurement Results from WD40A Piles

The second data measurements were made on 25 October 2014 when the main piles of WD40A were severed. Data were collected from 12 of the 12 sensors. The parameters describing these shots are shown in **Table 4**. The pressure results for each explosion are shown in **Figure 20**.

Again, there appear to be anomalous data points in the lower left-hand corner of these plots. These data were recorded on the near-bottom sensors A, D, and G. **Figure 21** shows the same data set with these three sensors removed. The correspondence to a linear relationship is much better among the remaining data channels.

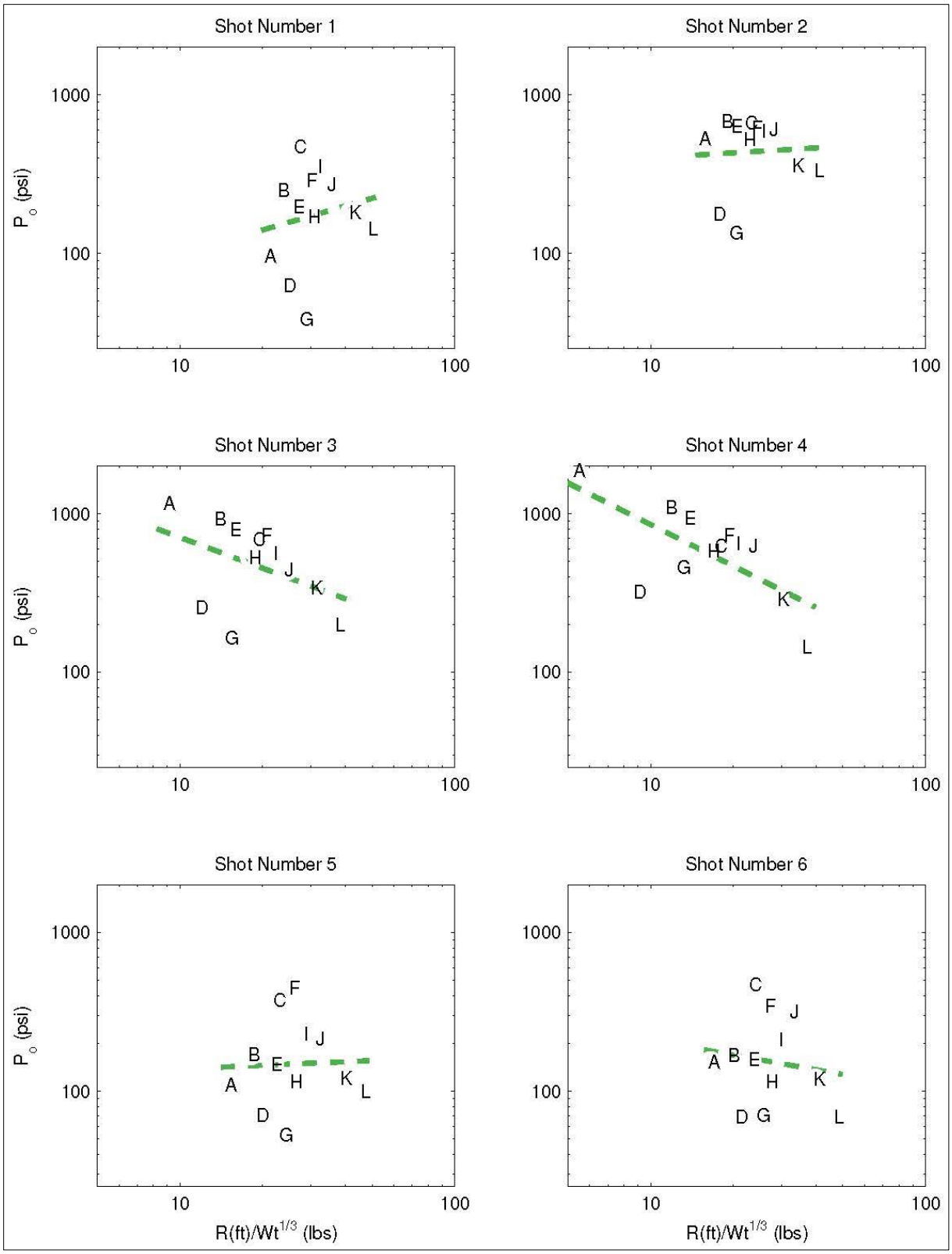

Figure 20. Pressure as a function of reduced range for the WD40A pile shots.

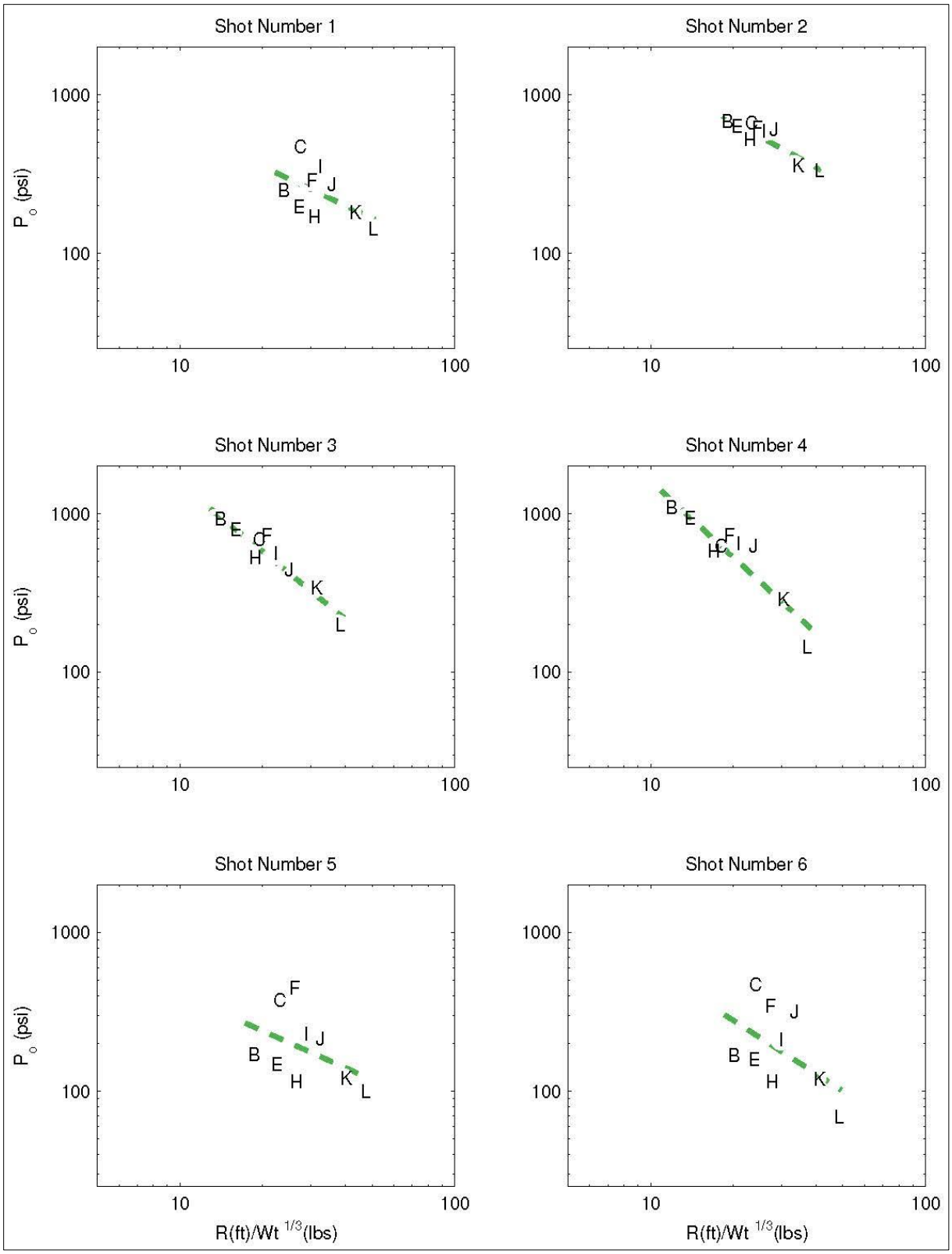

Figure 21. Pressure data from the WD40A main piles, with the three near-bottom sensors removed.

3.1.3 Measurements Results from WD40B Piles

The second structure was removed on 28 October 2014, when five of the six main piles were shot. One pile had an obstruction that did not allow for the BML placement of the explosive charge. Data were collected on all 12 sensors. The geometry of the main piles is shown in **Figure 22**, where the location of the piles in horizontal space is shown relative to the charge locations (measured in feet). Only five piles are illustrated, because one pile was not severed explosively. The parameters describing these shots are shown in **Table 4**. The pressure results for each explosion are shown in **Figure 23**.

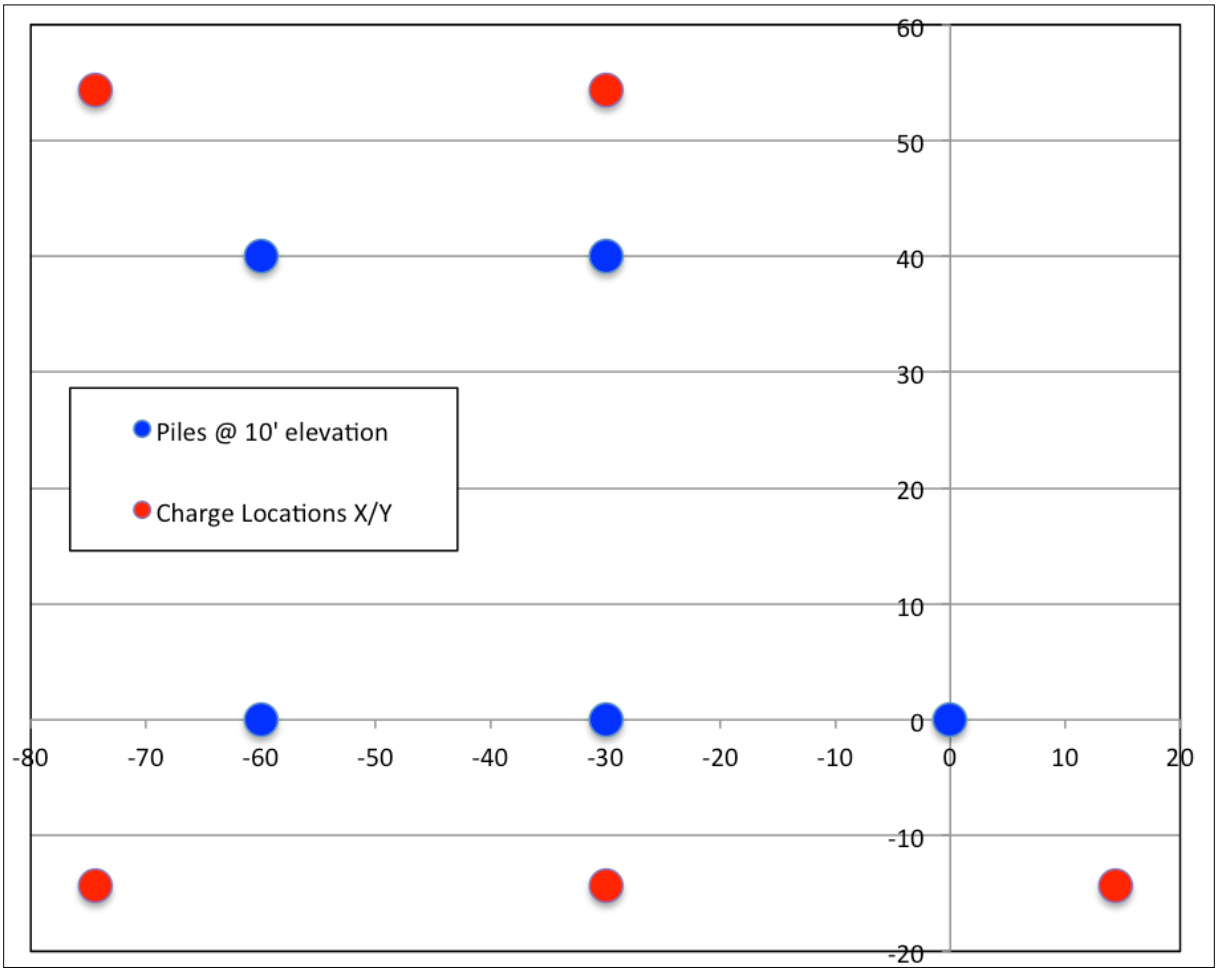

Figure 22. Top-down view of the positions of the five main piles and charge location for the WD40B platform.

The positions of the main piles are shown at the 10-ft elevation, as per the original plans. The positions of the BML charges were determined from the slope of the main piles (12.5%).

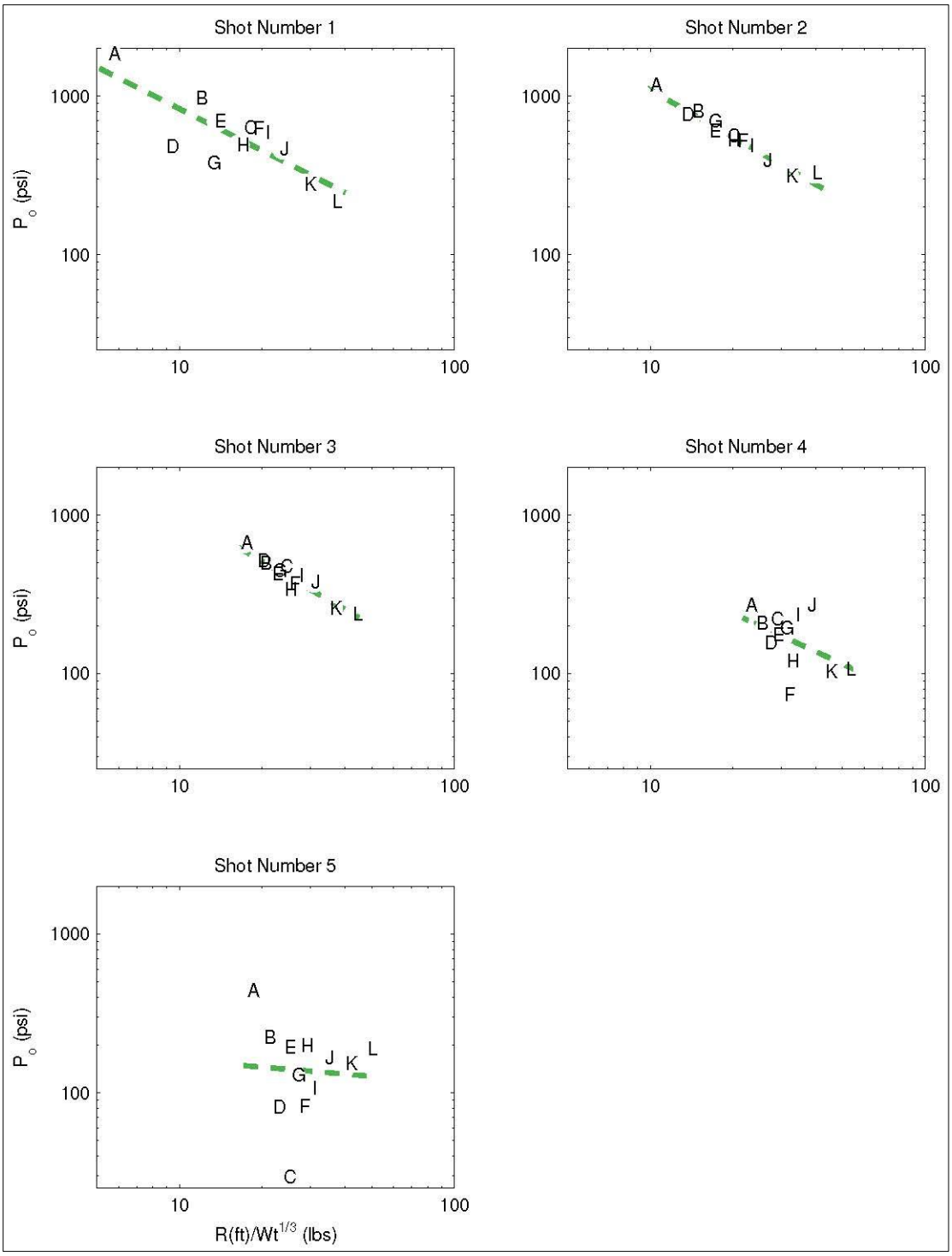

Figure 23. Measured peak pressure as a function of the reduced range axis for the WD40B pile shots.

The data from WD40B show fewer apparently anomalous data points. There was no consistent pattern as to which sensor produced the very low values. At the WD40A locations, all of the anomalously low values were measured with the near-bottom sensors. At WD40B, there was no such obvious pattern. The most aberrant points were those with values less than 100 psi. **Figure 24** presents these data with five points (<100 psi) removed.

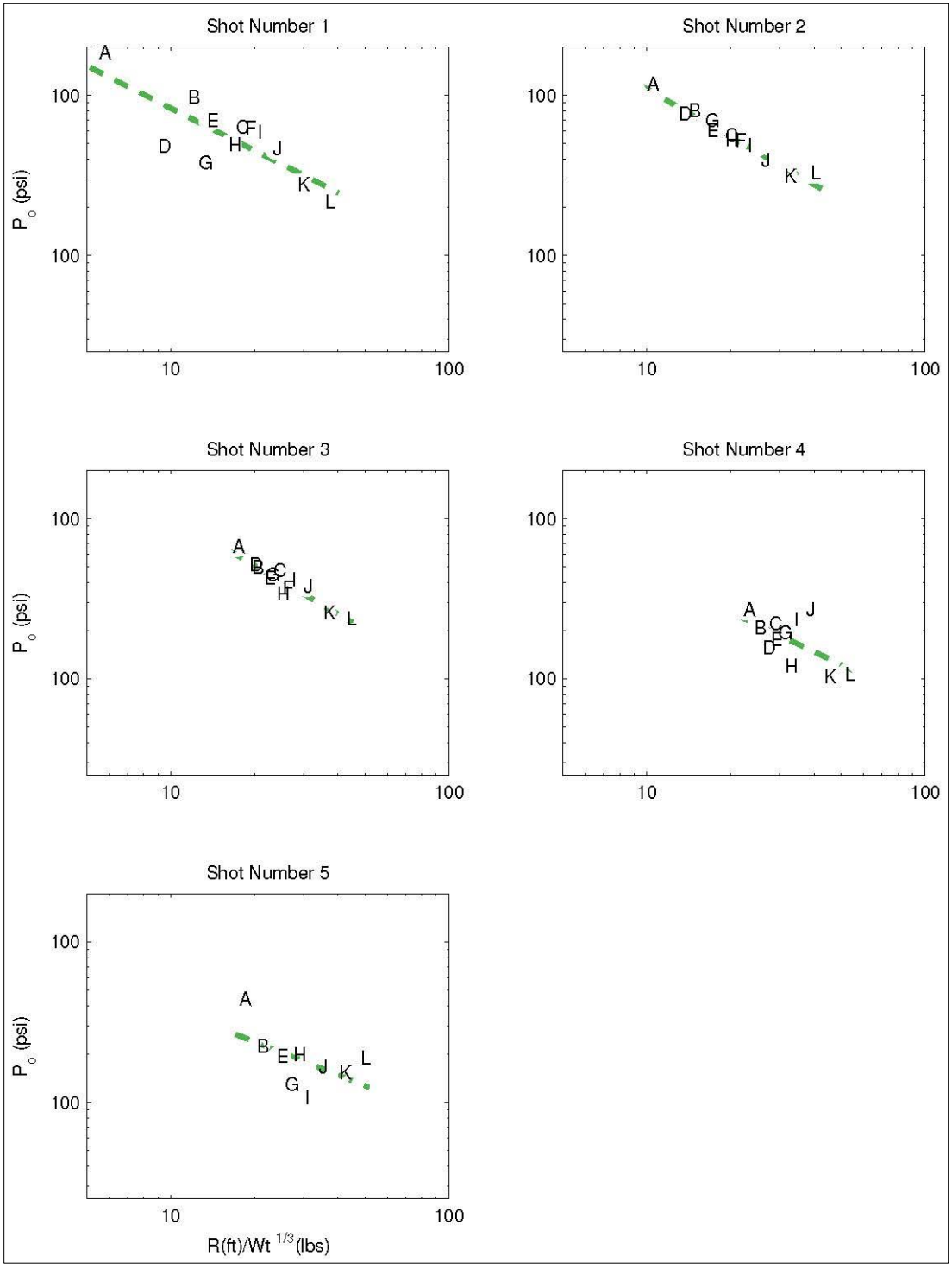

Figure 24. WD40B pressure data with values less than 100 psi removed.

All of the data from **Figures 21** and **23** were combined and are presented in **Figure 25.** A line was fit to the data (red line). The pressure dropped at a rate of $R^{-1.30}$, faster than the predictions of the UWCv1 ($R^{-1.13}$), but not as quickly as the predictions reported by UWCv2.

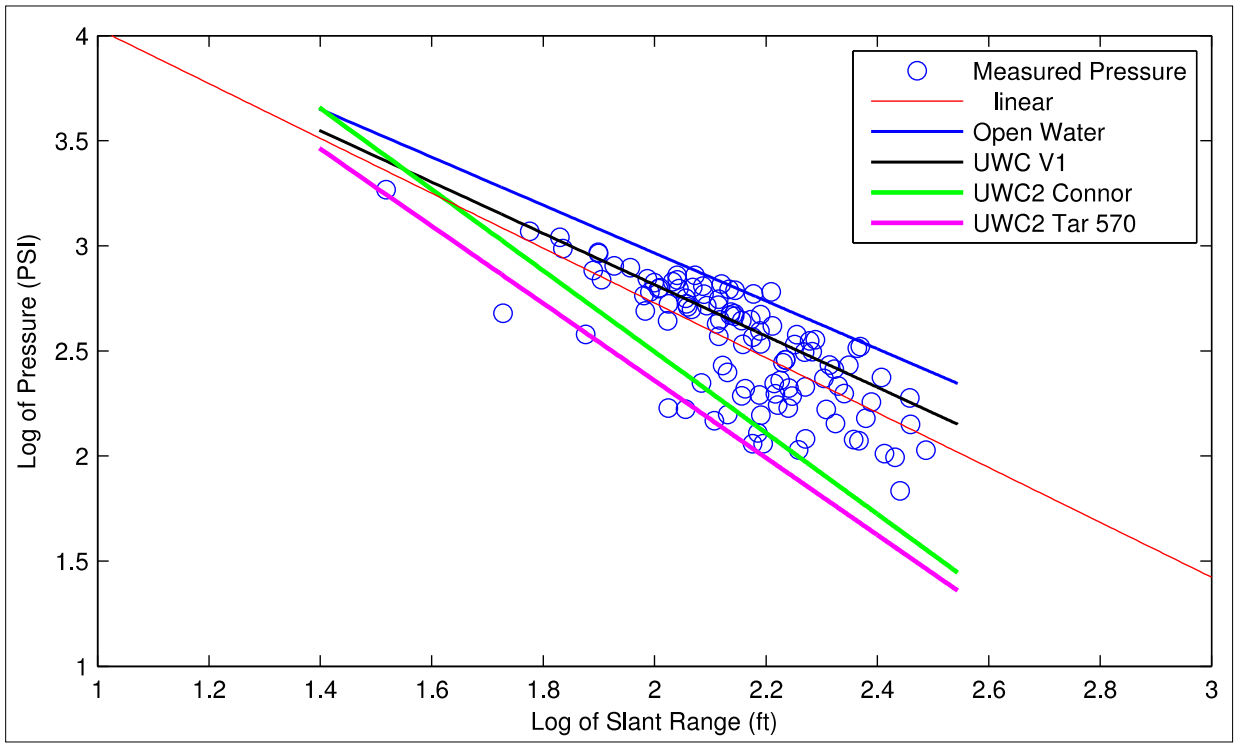

Figure 25. All of the 200-lb charge pressure data (with questionable values removed).

Note the strong correspondence between the line fit to the data and the predictions of the UWCv1. The data values are much closer to the UWCv1 predictions for the 200-lb charges than the 75- and 100-lb charges.

3.2 ANALYSIS OF MEASUREMENT RESULTS

The individual pressure time series (waveforms) differed considerably in detailed form from the theoretical predictions for exponential decay of an explosive signal. This condition had been noted in earlier work (Poe et al., 2009). It has been suggested that multiple reflections from the structure, and from the water surface, may contribute to this effect.

3.2.1 Peak Pressure

The previous sections have presented the pressure results for each shot from each explosive event. **Figures 26** and **27** present all of the data for each charge size. These figures showed that the measured decay rate with distance was a good match for both UWC predictions, although the amplitude was intermediate between the Version 1 and Version 2 (using TAR Project No. 570 input) predictions.

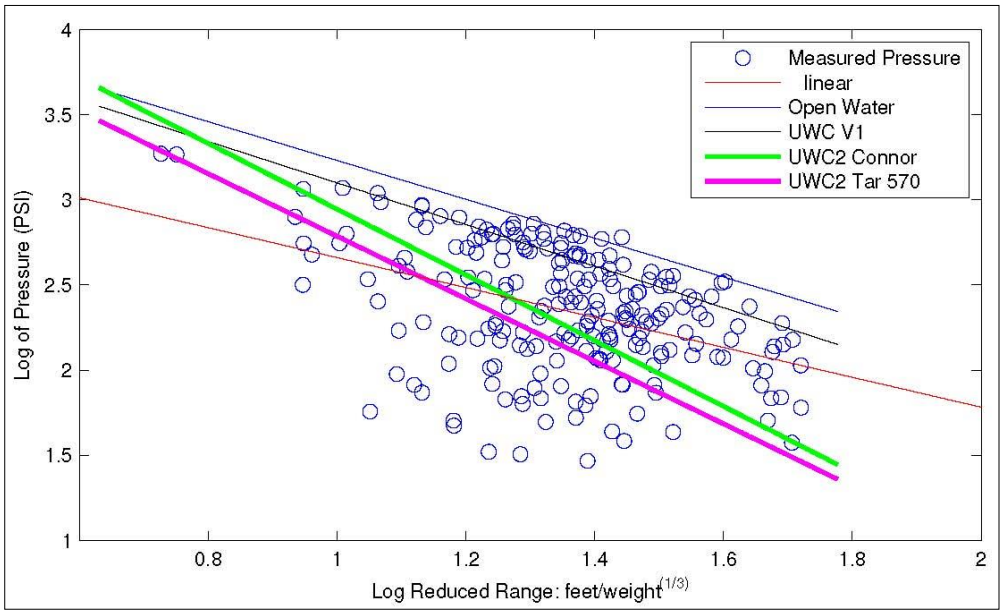

Figure 26. All pressure data as a function of the log scaled-weight axis.

The UWC predictions are shown as well as a linear fit to the log-log plot. The curve fit to the data parallels the decay rate of the open-water curve (**Figure 26**), but at a reduced amplitude.

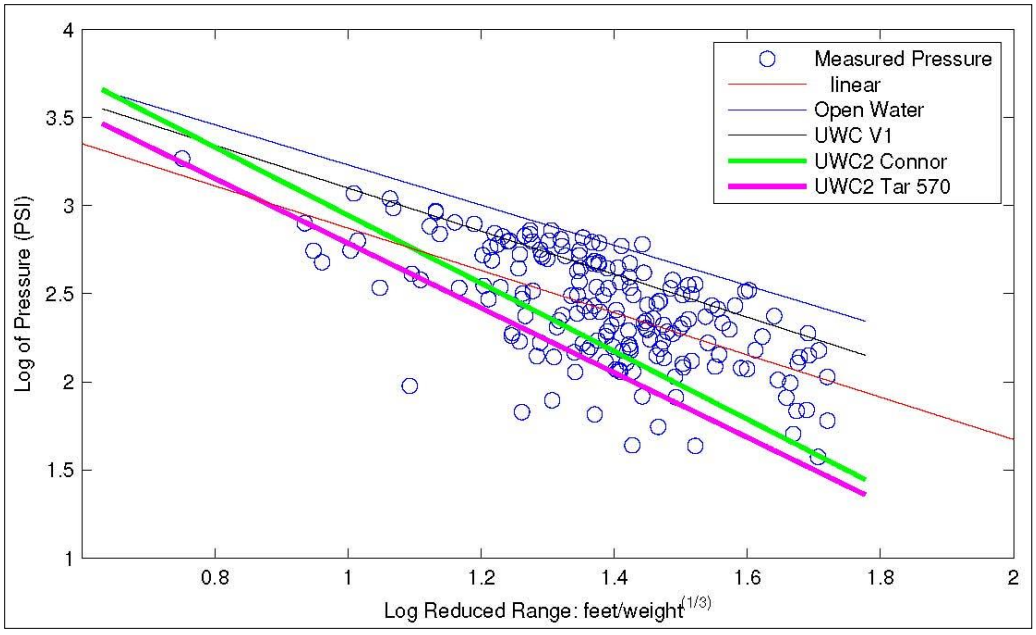

Figure 27. Curve-fit decay rate plots for combined data.

A more general view can be obtained by combining data, where appropriate. **Figure 28** shows the data for all charges, plotted as a function of the reduced-range (x-axis) of slant range/charge weight$^{1/3}$. The slope of the line fitted to those data was -0.8784, which indicates spreading rates intermediate between cylindrical and spherical. **Figure 29** shows the same data, with the questionable data points removed. Here the measured decay rate of the data is -1.199, only slightly greater than the 1.13 value predicted by the UWCv1, albeit at a slighted reduced amplitude. The UWCv2 predictions show a greater rate of attenuation with range than that shown by the data.

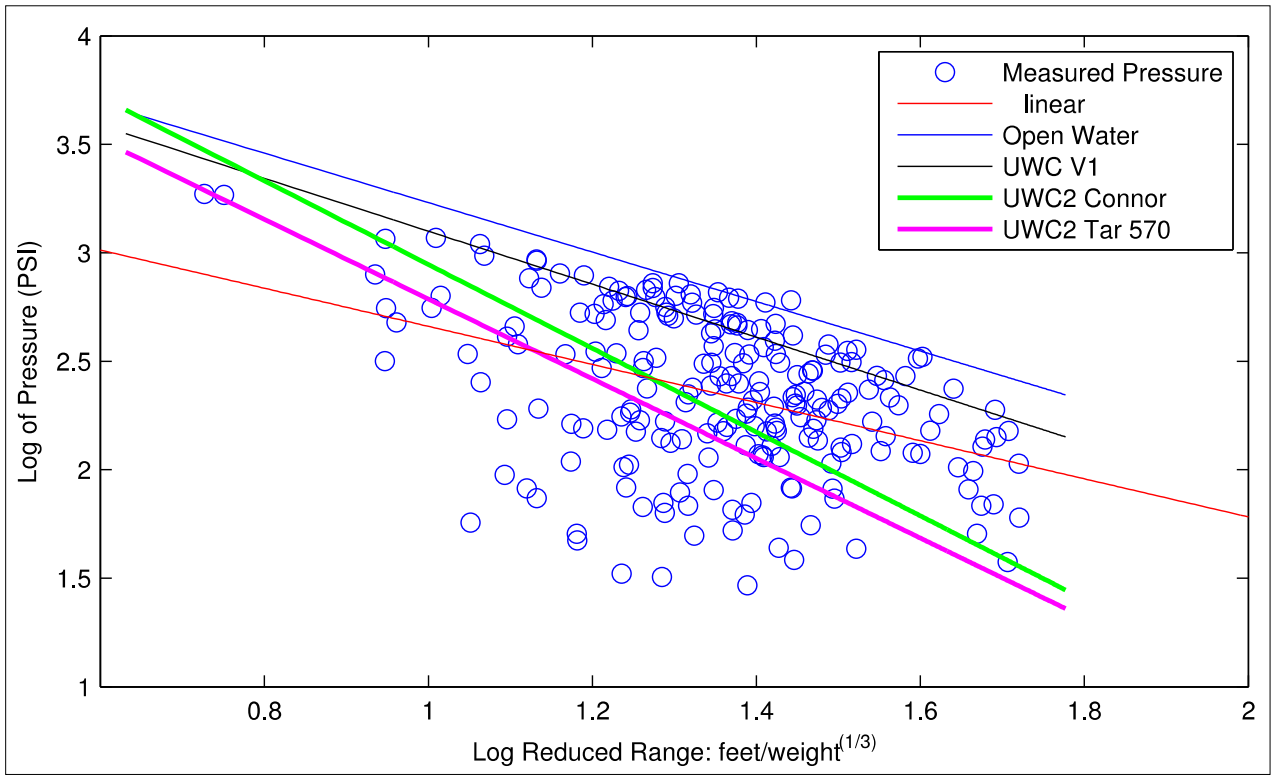

Figure 28. All pressure data as a function of the reduced range. Slope (red line) is -0.8784.

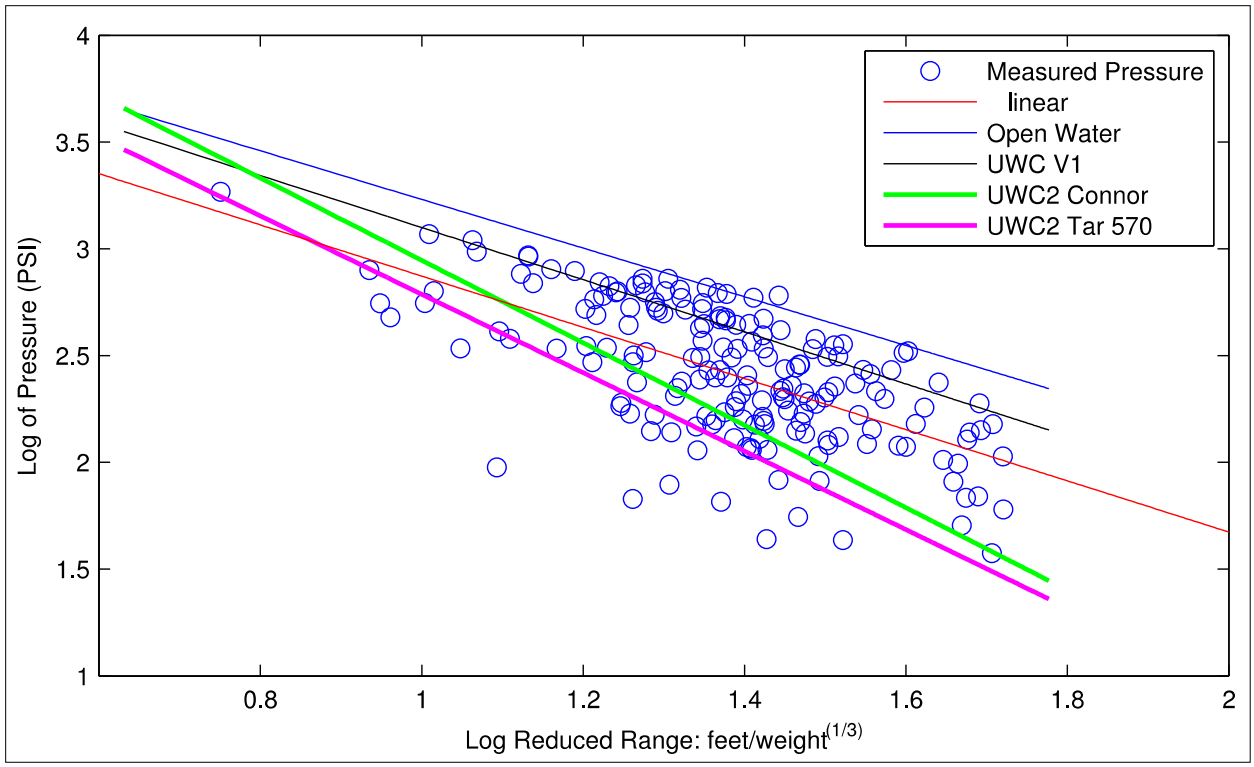

Figure 29. All pressure data as a function of the log scaled-weight axis, with the questionable data points removed. Slope (red line) is -1.199.

The measured values were compared with predictions from the UWCv2 for the well conductors and main piles, using the TAR 570, Connor, and open-water options (Dzwilewski, 2014). In both presentations of the pressure data, the curve fit to the data largely parallels that for the open-water predictions, albeit with what appears to be a near-constant offset with of the measured data having a lower amplitude.

3.2.2 Impulse Data

Figures 30 and **31** show the impulse data plotted as a function of the reduced range, with and without the suspect data points, respectively. As seen with the pressure data, the linear fit to impulse data has the same approximate slope (decay rate), as the predictions of the UWCv1. However, the amplitudes of the measured data are lower than the UWCv1 predictions.

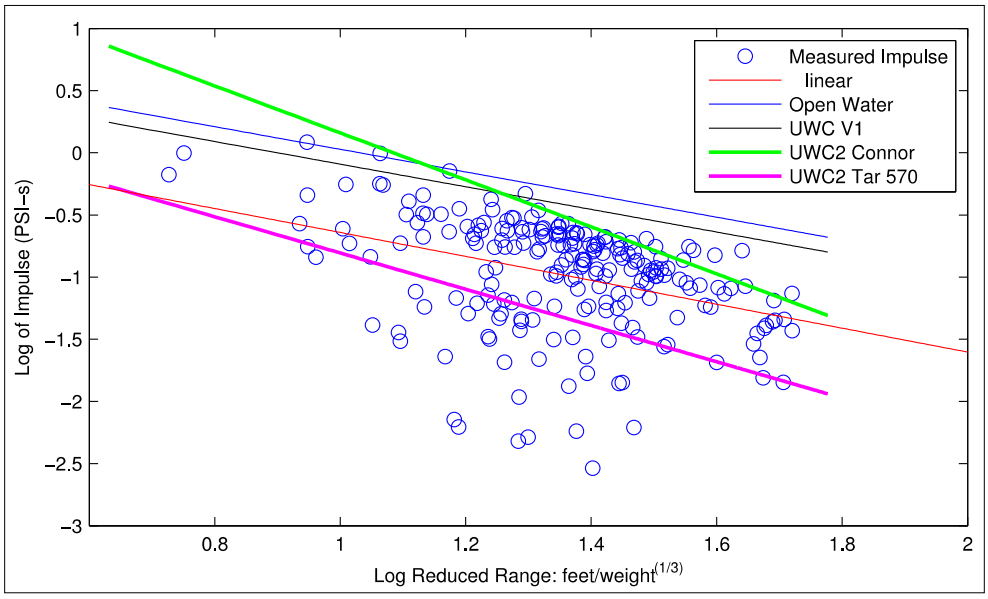

Figure 30. Impulse data plotted as a function of the reduced range.

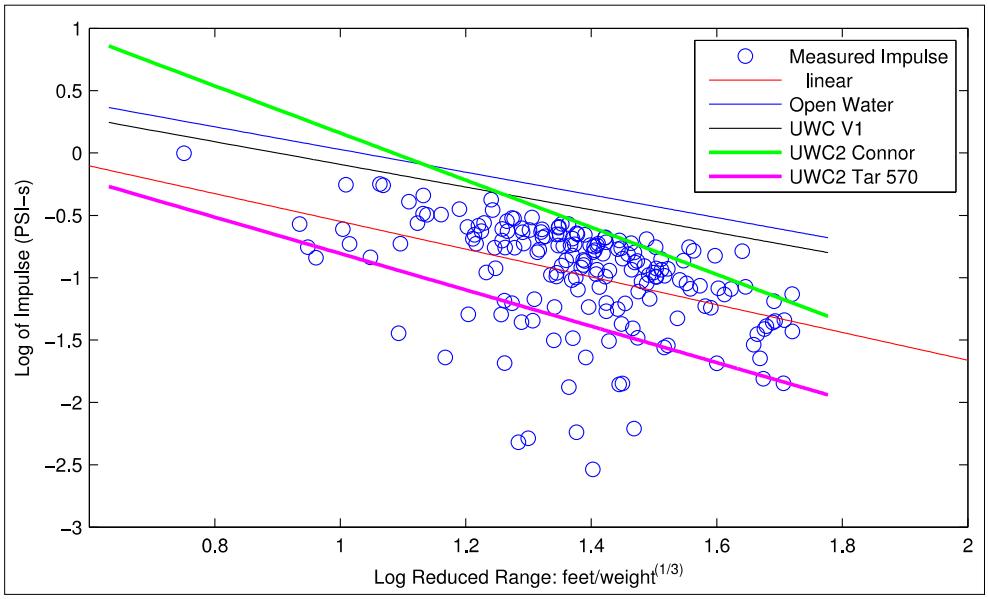

Figure 31. Impulse data plotted as a function of the reduced range, but with the questionable data points removed.

3.2.3 Energy Flux Density Data

The EFD data presented in **Figures 32** and **33** show the same trend as seen in the pressure data, with the curve fit to the data paralleling that of the UWCv1 predictions.

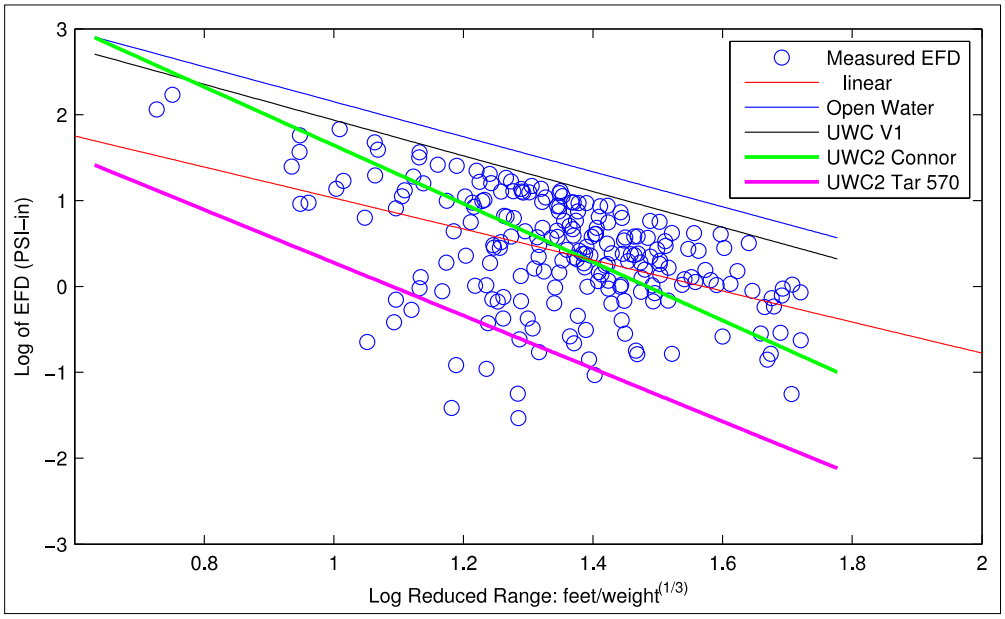

Figure 32. Energy flux density (EFD) plotted as a function of the reduced-range axis.

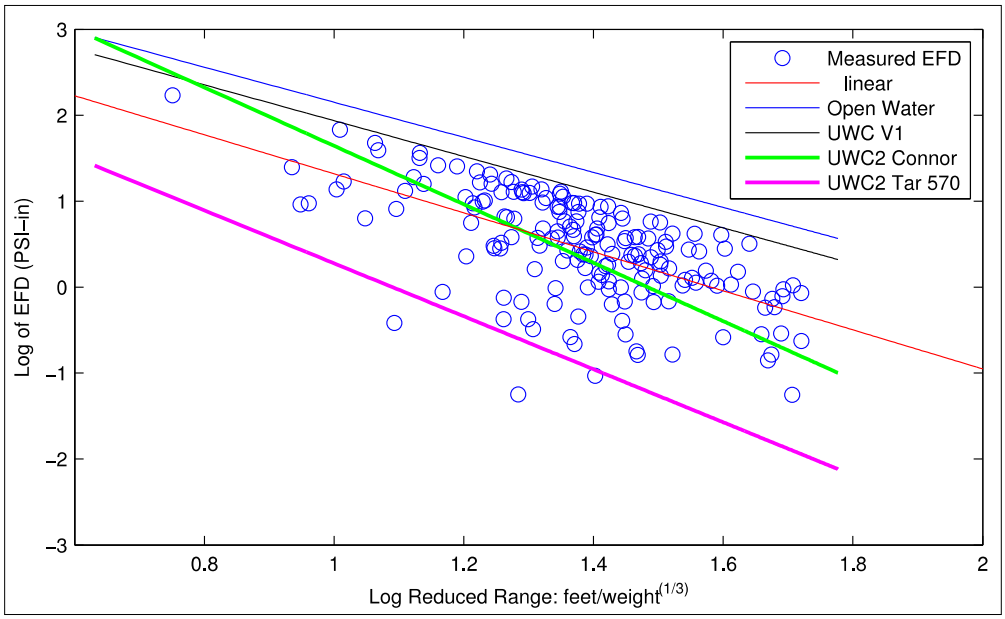

Figure 33. Energy flux density (EFD) plotted as a function of the reduced-range axis, but with the questionable data points removed.

4.0 DISCUSSION

There was considerable variability in the data, but clear trends were observed in comparisons of the measured data with the UWC (Versions 1 and 2) predictions. When measured data were compared with UWC predictions, the UWCv1 consistently overestimated the pressure levels and slightly underestimated decay rates for the 75- and 100-lb charges. However, the UWCv1 predictions showed a close fit for measured pressure levels and decay rates for all 200-lb charge data. The UWCv2 predictions produced a poor fit to the measured pressure values. The UWCv2 (Connor and TAR 570) predicted a faster decay rate as compared to the UWCv1 and the measured results.

Both forward and backward calculation Microsoft© Excel© spreadsheets are provided for UWCv1 and UWCv2 in **Appendix 1**. The variation of predicted results for the EFD and decay rates between UWCv1 and UWCv2 to the measured values is most likely due to the premise upon which each calculator was built. The inputs to UWCv2 have been simplified compared to the inputs required for UWCv1. Specifically, UWCv1 requires the user to input pile diameter and thickness, while the UWCv2 requires the user to select a scenario, such as "main pile Connor" or "well conductor TAR 570". These scenarios represent the type of structure being removed as well as the source of the measurement data (Connor or TAR 570). Despite these differences in inputs, the forward calculation in both versions still predicts the peak pressure, impulse, and energy flux density for an input slant range and explosive weight for a selected pile scenario, and these values provide the information necessary to calculate exclusion zones and take estimates.

The different required inputs stem from the premise upon which each calculator is built. The UWCv1 is based on near-field energy coupling from the physics of shock wave propagation (Dzwilewski and Fenton, 2003). These calculations use the physics of underwater propagation and the dampening effects of structural properties to theoretically calculate the near-field predictions. Those near-field predictions are also used in the far field. Conversely, the UWCv2 is based solely on curve-fits applied to the TAR 570 data and the Connor data (Dzwilewski, 2014). These curve-fit data are used for both the near-field and far-field calculations. The outputs from UWCv2 with either of these selected scenarios (Connor or TAR 570) will thus be driven specifically by the physical parameters of those individual project data sets and, therefore, may not be as universally applicable to all situations. This exact result is found when comparing the measured data from this study with the outputs of UWCv2. As such, the outputs of the two models (UWCv1 and UWCv2) differ markedly in their predicted attenuation rates (Dzwilewski, pers. comm.).

In some individual measurements, the recorded pressure value was higher at greater slant ranges (e.g., **Figure 19**, shot 1). This suggests a potential for error in individual measurements that must be considered during the interpretation of the data. Because most of the anomalous data points came from the near-bottom sensors, a number of factors may be at work in producing these results. The positioning of the sensor and interaction with the physical characteristics of the removal site likely have the greatest role in producing this anomaly. Each detonation is timed 1 to 2 s apart and will reach the array sensors along different pathways and, depending on the spatial relation to the sensors, will interact with other pressure waves (direct or reflected). Though individual variation is to be expected, the complexity of the pressure waves interacting with the substrate and the existing structure may create a shadowing effect where pressure may be dampened before reaching certain sensors, producing results that appear as "higher" peak pressures and EFD in sensors that are farther away (**Figure 34**) from the detonation. This is best exemplified in the better slope-fit for peak pressure versus slant range (fixed) between detonations that had no structure between the pile and the sensor (**Figure 20**, shot 4) compared to detonations that had piles, sonar reflectors, and other structures between the target pile and sensor (**Figure 20**, shot 1).

This is also seen in the relative consistency of good slope fit for all the near-surface sensors in the same figures. These assumptions hold true with and without the inclusion of sensors D and G, which likely show the complexity of interactions with the pressure waves for the lowest sensors. Specifically, there is less linear agreement between pressure measurements and slant range for piles that are

detonated later in the sequence and for those that have other structures between them and the sensor array.

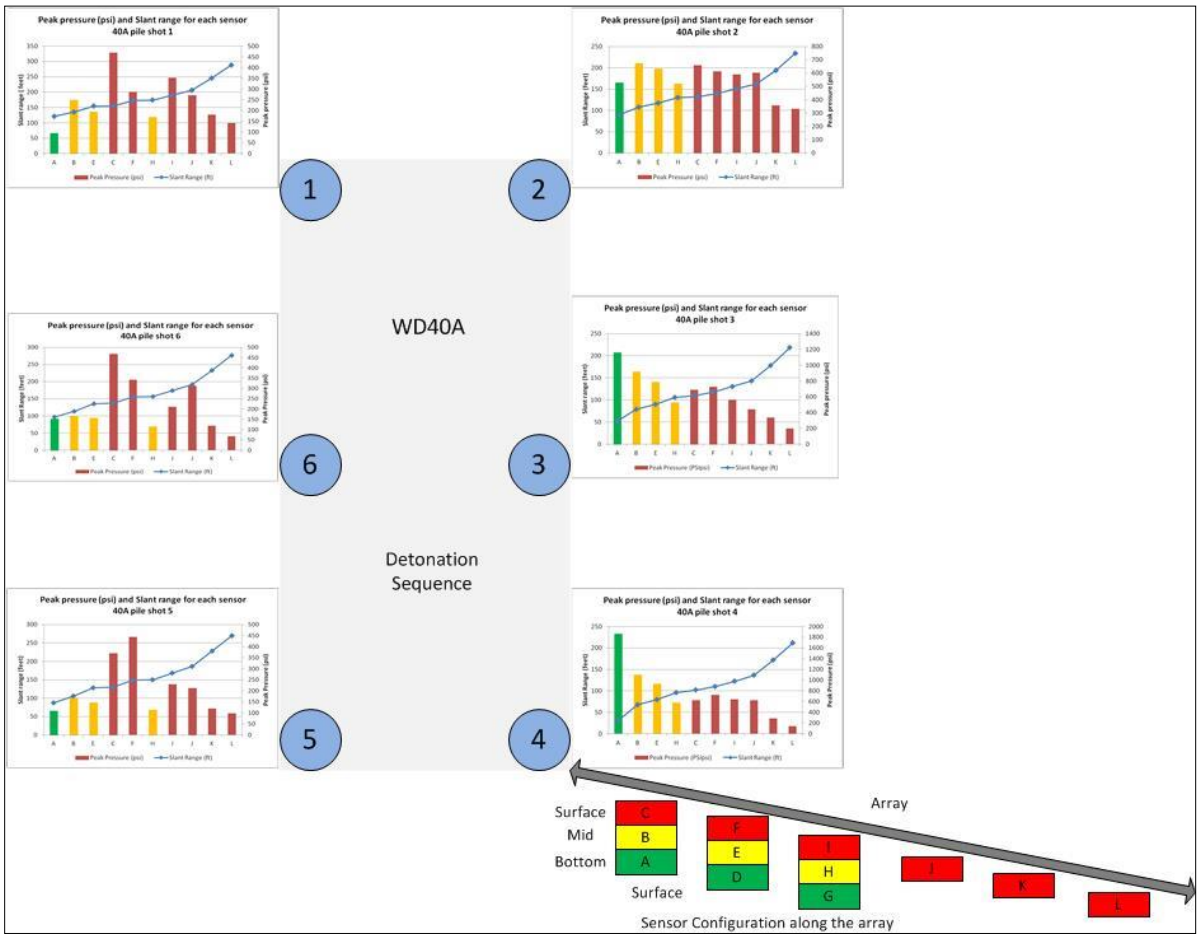

Figure 34. Sample detonation sequence (with sensors D and G removed) and pile location relative to sensor location.

Embedded graphs compare measured peak pressure (bar graph) to slant range (line graph). The bar graph color corresponds to the sensor location (surface, mid or bottom).

The water depths at the study sites were between 90 and 95 ft, almost twice as deep as the data collection efforts at the TAR 118 (Connor) and TAR 570 study sites. The difference in water depth may be related to the difference in the observed decay rates from the predictions that were based on the shallow water observations. The sediment type and characteristics were also different than at the previous study sites. Propagation of acoustic waves through a porous seabed depends on the type, distribution, density, and stress state of the sediments. The fundamental connection that exists between acoustic energy propagation and the physical and behavioral properties of the sediments is firmly established with the work of Hamilton and Bachman (1982), Bachman (1985), Richardson and Briggs (1993), and Wilkens (1998). Specifically, softer sediments will attenuate acoustic and pressure waves more effectively than harder sediments. However, the liquefied nature of the sediments found on the PWAP 40 sites may contribute to the inconsistency of the linear attenuation of the pressure wave.

It is not possible to quantify the specific contribution from suspended particles, water depth, structural interference, or other controlling factors, such as gas bubble entrapment. There is likely a synergistic effect among multiple factors that results in complex attenuation patterns in the near field.

Although it is beyond the scope of the current project to evaluate these hypotheses, these variables seem relevant and worthy of further investigation and perhaps modification of UWCv2.

However, these outlier values affected only the pressure results shown in **Figures 28** and **29**. The curve fit to all of the data points has a decay rate less than that for the open water. When those points are removed, the decay rate is very close to that predicted by the UWCv1 for pile constrained explosions (slopes of -1.19 and -1.13). The decay rates for impulse (**Figures 30** and **31**) and EFD (**Figures 32** and **33**) were not greatly affected by inclusion or removal of the suspect data points. This may result in part from the measurement process that removed any point for which a time constant could not be reliably measured.

The predictions of the two versions of the UWC differ markedly. UWCv2 predicts greater decay of amplitudes with range than UWCv1, which is based on numerical simulations of the shock wave propagation through the sediment. UWCv2 is based on empirical data from earlier experiments. However, there were notable differences between those two earlier experiments and the current work, including water depth, pile diameter, charge size, and depth BML (**Table 5**).

Table 3. Comparison of parameters of past and current studies.

Experiment	Water Depth (ft)	Charge Sizes (lb)	Depth BML (ft)	Wall Thickness (in.)
TAR 118 (Connor)	53	25–50	8–26	1.00
TAR 570	50	75–145	15–30	0.625–1.50
Current	92	75–200	15–25	1.00–2.25

5.0 CONCLUSIONS

Compared to this study, earlier studies (Connor and TAR 570) that are used for UWCv2 development took place in water that was about half as deep and used smaller charges that were often placed deeper than the current study BML level. UWCv1 is based on physics models, rather than curves fit to data from two specific locations that may vary greatly depending on project parameters. UWCv1 returned accurate predictions of the results from this study but overestimated the measurements from Connor and TAR 570 projects. But both the UWCv1 and UWCv2 predictions will produce safety ranges that are smaller than those for an open-water explosion.

The observed data from the current experiment were accurately predicted by UWCv1. As with the Connor and TAR 570 data, the UWCv1 generally over-predicted the actual measured PWAP levels.

The UWCv2 was built on curves fit to the data from TAR 570 and the Connor experiments. The UWCv2 predictions had a quicker decay rate with range than the UWCv1 predictions and the observed data from the current study. These results suggest that the effects of the differing parameter combinations are not fully incorporated into the UWCv2. The current study was conducted in deeper water and used larger charge sizes than either the Connor or TAR 570 project.

All predicted and measured pressure level data for the BML detonations were lower than the predicted amplitudes of an open-water charge for all charge weights, indicating that using an open-water model calculation to establish take or safety zones would consistently overestimate the size of the impact area for detonations at any charge weight or depth BML. Conservative estimates from both UWCv1 and UWCv2 provide impact zone predictions that remain far below calculations for an open-water blast.

The implications for using either UWC to determine exclusion zones and impact assessment from decommissioning events lie in the utility of these calculators in predicting the impulse, EFD, and peak pressure at given distances from the platform. For impulse, EFD, and peak pressure, the measured attenuation was consistently better fit to the predicted values produced by the UWCv1 than by the UWCv2. Measured peak pressures were consistently lower than those predicted by UWCv1, but were variable compared to UWCv2; closer distances were over predicted and farther distances were under predicted. UWCv1 provides a consistently more conservative and accurate prediction of measured values important in impact evaluation.

Regulatory use of the UWC involves the backward calculation that calculates the slant range for the input (e.g., Level B take criteria for pressure and energy flux density values for different open-water and pile scenarios).

The objective of this study was to quantitatively measure the underwater pressure waves and acoustic proprieties generated by the detonation of explosives used for severance during offshore structure removal ops and provide BSEE and BOEM with scientifically valid data to update the ARA model so that the take harassment impact zones of protected species may be more accurately calculated. Data collection was needed to further document the dampening effects of the target structures and surrounding sediments; particularly by deepening the severance depth or making severance cuts internal to larger tubulars (i.e., cutting conductors in caissons or large jacket legs).

This study advanced the understanding of the underwater pressure waves and acoustic properties of severance-charge detonations under varying physical conditions. Charge weights were greater than for previous studies, water depth was greater than previous studies, and overall, wall thickness of the structures was generally larger than in previous studies. The dampening effects of sediment differences were also considered as a contributing factor in the resulting UWC calculations for this study when compared to previous studies. Charge depth within the structure and alternative methodologies of severance were not explored fully due to the operational parameters of the available target structures.

The field measurements from this study and their predicted calculations using UWCv1 and UWCv2 show that UWCv1 provides a more accurate and conservative prediction of impact criteria. Peak pressure (psi) and EFD are the dual criteria typically used by NMFS in determining impact zones and take estimates for marine mammals and sea turtles from explosive sources. Measured psi values during

this study were generally lower than those predicted by the UWCv1 and were always lower than unconfined, open-water predictions for either UWCv1 or UWCv2. UWCv1 can be safely and conservatively used universally for impact assessment and survey planning, while UWCv2 could be used in some circumstances, namely for removals conducted near the TAR 570 or Connor study sites and with charge sizes that are no larger than 80 lb. UWCv2 is ideally the calculator version that should be applied in regulatory frameworks, because it uses project-specific information. However, based on this study, further refining of the UWCv2 is needed to achieve better agreement with EFD rates on a consistent basis. The data collected during this study can be applied for updating the UWCv2 model.

6.0 LITERATURE CITED

Arons, A.B., D.R. Yennie, and T.P. Cotter. 1950. Long range shock propagation in underwater explosion phenomena II. In: Underwater Explosions: A Compendium of American and British Reports, Vol I, The Shock Wave. Office of Naval Research, Washington, DC.

U.S. Dept. of the Interior. Bureau of Safety and Environmental Enforcement. 2016. Offshore Statistics by Water Depth. Available at: www.data.bsee.gov/homepg/data_center/leasing/WaterDepth/WaterDepth.asp.

Bachman, Richard T. 1985. Acoustic and physical property relationships in marine sediment. The Journal of the Acoustical Society of America 78(2):616-621.

Connor, Jr., J. 1990. Underwater blast effects from explosive severance of offshore platform legs and well conductors. Naval Surface Warfare Center, Silver Spring, MD. NAVSWC TR 90-532. U.S. Dept. of the Interior, Minerals Management Service, Technology Assessment and Research (TAR) Program, Herndon, VA. [TAR Project No. 118]

Continental Shelf Associates, Inc. 2004. Explosive removal of offshore structures – information synthesis report. U.S. Dept. of the Interior, Minerals Management Service, Gulf of Mexico OCS Region, New Orleans, LA. OCS Study MMS 2003-070.

Department of the Navy. 1998. Final environmental impact statement: Shock Testing the Seawolf Submarine. U.S. Department of the Navy, Southern Division, Naval Facilities Engineering Command, North Charleston, SC.

Department of the Navy. 2001. Shock Trial of the Winston S. Churchill (DDG 81): Final environmental impact statement. Department of the Navy, Naval Sea Systems Command. Washington, D.C.

Dzwilewski, P. and G. Fenton. 2003. Shock Wave/Sound propagation modeling results for calculating marine protected species impact zones during explosive removal of offshore structures. Applied Research Associates, Inc., Kenner, LA, January 20, 2003.

Dzwilewski, P.T. 2014. Water Shock Prediction For Explosive Removal Of Offshore Structures: Underwater Calculator (UWC) Version 2.0 Update Based Upon Field Data.

Federal Register. 2008. Taking and importing marine mammals; taking marine mammals incidental to the explosive removal of offshore structures in the Gulf of Mexico. 73FR34875, pp. 34875-34894.

Federal Register. 2014. Takes of marine mammals during specified activities; confined blasting operations by the US Army Corps of Engineers during the Port of Miami construction project in Miami, FL. 79 FR6545, pp. 6545-6567.

Frankel, A., and W. Ellison. 2004. Explosive removal model simulation report. U.S. Dept. of the Interior, Minerals Management Service, Gulf of Mexico OCS Region, New Orleans, LA. OCS Study MMS 2004-064.

Hamilton, Edwin L., and R.T. Bachman. 1982. Sound velocity and related properties of marine sediments. The Journal of the Acoustical Society of America 72(6):1891-1904.

Kaiser, M.J., D.V. Mesyanzhinov, and A.G. Pulsipher. In preparation. Modeling structure removal processes in the Gulf of Mexico. U.S. Department of the Interior, Minerals Management Service, Gulf of Mexico OCS Region, New Orleans, LA.

Mathworks. 2014. Matlab. Cambridge, MA.

National Oceanic and Atmospheric Administration. 2006. Biological Opinion: Permitting Structure Removal Operations on the Gulf of Mexico Outer Continental Shelf. 133 pp.

Poe, W.T., C.F. Adams, R. Janda, and D. Kirklewsiki. 2009. Effect of Depth Below Mudline of Charge Placement During Explosive Removal of Offshore Structures (EROS) – final report. U.S. Dept. of the Interior, Minerals Management Service, Technology Assessment and Research (TAR) Program, Herndon, VA (TAR Project No. 570).

Richardson, M.D., and K.B. Briggs. 1993. On the use of acoustic impedance values to determine sediment properties. Final Report No. NRL/PP/7431-92-0001. Naval Research Lab, Stennis Space Center, MS. 12 pp.

Richardson, W.J., C.R. Greene, Jr., C.I. Malme, and D.H. Thomson. 1995. Marine Mammals and Noise. Academic Press, San Diego, CA. 576 pp.

Saint-Arnaud, D., P. Pelletier, W. Poe, and J. Fowler. 2004. Oil platform removal using engineered explosive charges: In-situ comparison of engineered and bulk explosive charges – final report. U.S. Dept. of the Interior, Minerals Management Service, Technology Assessment and Research (TAR) Program, Herndon, VA. [TAR Project No. 429]

Swisdak, M.M., Jr. 1978. Explosion Effects and Properties: Part II - Explosion Effects in Water. Naval Surface Weapons Center, 22 February 1978.

Urick, R.J. 1983. Principles of Underwater Sound, 3rd edition. McGraw-Hill, New York. 423 pp.

U.S. Dept. of the Interior. Minerals Management Service. 2005. Structure-removal operations on the Outer Continental Shelf of the Gulf of Mexico—Programmatic environmental assessment. U.S. Dept. of the Interior, Minerals Management Service, Gulf of Mexico OCS Region, New Orleans, LA. OCS EIS/EA MMS 2005-013. 333 pp. Available at: http://www.nmfs.noaa.gov/pr/pdfs/permits/mms2005_013.pdf Accessed February 8, 2016.

Wilkens, R.H., and M.D. Richardson. 1998. The influence of gas bubbles on sediment acoustic properties: in situ, laboratory, and theoretical results from Eckernförde Bay, Baltic Sea. Continental Shelf Research 18(14):1859-1892.

Appendix 1

WD40A Conductor Shot 1															
Sensor and Charge Data			Measured Data							ARA UWCv2 Data					
Sensor	Sensor Depth (ft)	Slant Range (ft)	Peak Pressure (Mpa)	Impulse (kPa·s)	EFD (kPa·m)	Peak Pressure (psi)	Impulse (psi·s)	EFD (psi·in.)	Time Constant (s)	Peak Pressure (Mpa)	Impulse (kPa·s)	EFD (kPa·m)	Peak Pressure (psi)	Impulse (psi-s)	EFD (psi-in.)
A	5	62.00	2.350	0.001	0.776	340.773	0.131	4.433	0.000	2.641	6.764	4.151	382.943	0.981	23.701
B	45	88.56	1.650	0.001	0.829	239.293	0.192	4.735	0.001	1.386	3.447	1.235	201.026	0.500	7.050
C	80	118.19	1.392	0.001	0.597	201.960	0.177	3.409	0.001	0.823	1.998	0.463	119.345	0.290	2.643
D	5	72.97	0.709	0.000	0.063	102.821	0.036	0.361	0.014	1.967	4.971	2.385	285.274	0.721	13.620
E	45	96.56	1.037	0.001	0.460	150.454	0.136	2.629	0.001	1.186	2.928	0.920	171.948	0.425	5.254
F	80	124.30	1.066	0.001	0.411	154.571	0.146	2.348	0.018	0.751	1.817	0.390	108.960	0.263	2.227
G	5	88.92	0.343	0.002	0.216	49.692	0.341	1.232	0.016	1.376	3.421	1.218	199.577	0.496	6.954
H	45	109.12	1.036	0.001	0.237	150.260	0.093	1.351	0.001	0.951	2.324	0.607	137.871	0.337	3.467
I	80	134.28	0.873	0.001	0.310	126.605	0.118	1.771	0.001	0.654	1.570	0.300	94.759	0.228	1.712
J	80	150.20	0.842	0.001	0.224	122.135	0.092	1.278	0.013	0.534	1.270	0.205	77.396	0.184	1.170
K	80	186.28													
L	80	221.60	0.415	0.000	0.041	60.213	0.037	0.234	0.001	0.264	0.609	0.055	38.326	0.088	0.312

WD40A Conductor Shot 2															
Sensor and Charge Data			Measured Data							ARA UWCv2 Data					
Sensor	Sensor Depth Above Mudline (ft)	Slant Range (ft)	Peak Pressure (Mpa)	Impulse (kPa·s)	EFD (kPa·m)	Peak Pressure (PSIpsi)	Impulse (psi·s)	EFD (psi·in)	Time constant (sec)	Peak Pressure (Mpa)	Impulse (kPa·s)	EFD (kPa·m)	Peak Pressure (PSIpsi)	Impulse (psi-s)	EFD (psi-in)
A	5	57.866	2.82864	0.1872	1.4234	410.259	0.1872	8.128	2.075	3.55741	10.167	8.0018	515.824	1.4746	45.692
B	45	85.723	1.63235	0.2362	1.1404	236.752	0.2362	6.512	2.805	1.74874	4.8374	2.1033	253.568	0.7016	12.01
C	80	116.08	1.09571	0.1822	0.6631	158.919	0.1822	3.7863	1.845	1.01123	2.7278	0.7504	146.629	0.3956	4.2852
D	5	71.701	1.07195	0.0062	0.0213	155.474	0.0062	0.1218	0.005	2.41491	6.78	3.8605	350.162	0.9834	22.044
E	45	95.609	1.41249	0.1601	0.6572	204.864	0.1601	3.7528	2.85	1.43574	3.9358	1.4513	208.183	0.5708	8.2869
F	80	123.56	1.04074	NaN	NaN	150.946	NaN	NaN	NaN	0.90332	2.4241	0.6069	130.981	0.3516	3.4654
G	5	90.184	0.43666	0.0459	0.2313	63.3326	0.0459	1.3208	6.24	1.59557	4.3952	1.7701	231.358	0.6375	10.107
H	45	110.15	1.18377	0.1003	0.3624	171.691	0.1003	2.0691	1.445	1.11164	3.0117	0.8968	161.188	0.4368	5.1207
I	80	135.12	0.97099	0.1156	0.405	140.83	0.1156	2.3128	3.765	0.76844	2.0469	0.4477	111.424	0.2969	2.5563
J	80	152.48	0.90755	0.1039	0.2903	131.629	0.1039	1.6575	2.715	0.6177	1.6289	0.2968	89.566	0.2363	1.695
K	80	190.45	NaN	NaN	NaN	NaN	NaN	NaN	NaN	0.41329	1.07	0.1394	59.9272	0.1552	0.7958
L	80	226.89	0.47834	0.0437	0.0505	69.3769	0.0437	0.2886	1.78	0.30123	0.7686	0.0769	43.6778	0.1115	0.4389

WD40A Conductor Shot 3															
Sensor and Charge Data			Measured Data							ARA UWCv2 Data					
Sensor	Sensor Depth Above Mudline (ft)	Slant Range (ft)	Peak Pressure (Mpa)	Impulse (kPa·s)	EFD (kPa·m)	Peak Pressure (PSIpsi)	Impulse (psi·s)	EFD (psi·in)	Time constant (sec)	Peak Pressure (Mpa)	Impulse (kPa·s)	EFD (kPa·m)	Peak Pressure (PSIpsi)	Impulse (psi-s)	EFD (psi-in)
A	5	51.824	2.35528	0.146	1.1048	341.605	0.146	6.3084	1.555	4.34188	12.523	11.642	629.573	1.8163	66.478
B	45	81.766	1.26149	0.1741	0.5304	182.964	0.1741	3.0285	4.26	1.90465	5.2894	2.4699	276.174	0.7672	14.104
C	80	113.18	0.89597	0.1389	0.2931	129.95	0.1389	1.6739	3.23	1.05839	2.861	0.8176	153.466	0.415	4.6688
D	5	62.927	0.50915	0.2108	0.1675	73.846	0.2108	0.9564	11.695	3.05732	8.6771	6.0172	443.312	1.2585	34.359
E	45	89.218	0.96449	0.0048	0.0099	139.888	0.0048	0.0566	0.005	1.62695	4.4856	1.8361	235.907	0.6506	10.485
F	80	118.68	0.80214	0.1071	0.203	116.34	0.1071	1.1593	3.14	0.9715	2.6158	0.6959	140.867	0.3794	3.9738
G	5	79.861	0.22902	0.0332	0.0193	33.2164	0.0332	0.1102	1.9	1.98754	5.5304	2.6761	288.194	0.8021	15.281
H	45	101.87	0.78365	0.0581	0.1702	113.658	0.0581	0.972	2.775	1.28022	3.491	1.1697	185.632	0.5063	6.6789
I	80	128.46	0.57066	0.056	0.1744	82.7677	0.056	0.9961	5.34	0.84193	2.2521	0.5316	122.079	0.3266	3.0355
J	80	144.37	0.5636	0.0675	0.1179	81.7426	0.0675	0.6731	1.61	0.68184	1.8063	0.3575	98.867	0.262	2.0413
K	80	180.84	NaN	NaN	NaN	NaN	NaN	NaN	NaN	0.45385	1.18	0.1662	65.8076	0.1711	0.949
L	80	216.64	0.34974	0.0226	0.0247	50.725	0.0226	0.1409	2.475	0.32745	0.8387	0.0899	47.48	0.1216	0.5135

WD40A Conductor Shot 4															
Sensor and Charge Data			Measured Data							ARA UWCv2 Data					
Sensor	Sensor Depth Above Mudline (ft)	Slant Range (ft)	Peak Pressure (Mpa)	Impulse (kPa·s)	EFD (kPa·m)	Peak Pressure (PSIpsi)	Impulse (psi·s)	EFD (psi·in)	Time constant (sec)	Peak Pressure (Mpa)	Impulse (kPa·s)	EFD (kPa·m)	Peak Pressure (PSIpsi)	Impulse (psi-s)	EFD (psi-in)
A	5	46.836	3.84132	0.245	2.4137	557.137	0.245	13.782	2.035	5.21314	15.163	16.424	755.906	2.1992	93.781
B	45	78.699	2.37114	0.2754	1.7271	343.905	0.2754	9.8619	3.695	2.04087	5.6857	2.8128	295.927	0.8246	16.061
C	80	110.99	1.72346	0.0803	0.4553	249.967	0.0803	2.6	0.005	1.09652	2.9689	0.8739	158.995	0.4306	4.9903
D	5	61.196	0.56509	0.0764	0.0933	81.9591	0.0764	0.533	3.615	3.21535	9.1467	6.6157	466.225	1.3266	37.777
E	45	88.005	2.26389	0.1739	1.0918	328.35	0.1739	6.2345	2.675	1.66766	4.6031	1.9236	241.811	0.6676	10.984
F	80	117.77	1.5736	0.1775	0.7197	228.231	0.1775	4.1098	3.06	0.98508	2.6541	0.7143	142.837	0.3849	4.079
G	5	80.904	0.57102	0.0873	0.3278	82.8196	0.0873	1.8719	6.01	1.9415	5.3965	2.5606	281.517	0.7827	14.621
H	45	102.69	2.14673	0.1095	0.6588	311.356	0.1095	3.7619	1.715	1.26182	3.4386	1.1382	182.964	0.4987	6.4994
I	80	129.11	1.48946	0.0139	0.0711	216.028	0.0139	0.4061	0.005	0.83427	2.2307	0.5225	120.97	0.3235	2.9838
J	80	146.43	1.39076	0.1096	0.4728	201.712	0.1096	2.6997	2.495	0.66457	1.7585	0.3406	96.363	0.255	1.9451
K	80	184.77	NaN	NaN	NaN	NaN	NaN	NaN	NaN	0.43656	1.133	0.1545	63.3008	0.1643	0.8822
L	80	221.67	0.95276	0.0409	0.1026	138.186	0.0409	0.5857	1.39	0.31416	0.8031	0.0832	45.5532	0.1165	0.475

WD40A Conductor Shot 5															
Sensor and Charge Data			Measured Data							ARA UWCv2 Data					
Sensor	Sensor Depth Above Mudline (ft)	Slant Range (ft)	Peak Pressure (Mpa)	Impulse (kPa·s)	EFD (kPa·m)	Peak Pressure (PSIpsi)	Impulse (psi·s)	EFD (psi·in)	Time constant (sec)	Peak Pressure (Mpa)	Impulse (kPa·s)	EFD (kPa·m)	Peak Pressure (PSIpsi)	Impulse (psi-s)	EFD (psi-in)
A	5	41.217	3.82985	0.176	1.6128	555.472	0.176	9.2094	1.115	6.56741	19.305	25.362	952.275	2.8	144.82
B	45	75.491	2.0324	0.2046	0.9814	294.775	0.2046	5.6036	3.38	2.20031	6.1511	3.2404	319.045	0.8921	18.503
C	80	108.74	1.86328	0.1509	0.6877	270.246	0.1509	3.9268	1.85	1.13789	3.0861	0.937	164.994	0.4476	5.3505
D	5	52.265	0.39385	0.0412	0.0395	57.123	0.0412	0.2256	2.985	4.27586	12.324	11.311	619.999	1.7874	64.588
E	45	82.047	1.31136	0.1193	0.4951	190.197	0.1193	2.8273	3.335	1.8929	5.2553	2.4413	274.471	0.7622	13.94
F	80	113.39	1.25093	0.1264	0.4199	181.432	0.1264	2.3976	3.745	1.05497	2.8513	0.8127	152.97	0.4135	4.6405
G	5	70.413	0.34933	NaN	NaN	50.6661	NaN	NaN	NaN	2.4953	7.0162	4.1059	361.819	1.0176	23.445
H	45	94.647	0.9541	0.0673	0.2843	138.381	0.0673	1.6231	2.395	1.46222	4.0117	1.502	212.022	0.5819	8.5767
I	80	122.81	1.12641	0.102	0.3204	163.373	0.102	1.8294	3.345	0.91321	2.4519	0.6194	132.416	0.3556	3.5371
J	80	138.57	0.94114	0.0772	0.2201	136.501	0.0772	1.2569	2.595	0.73425	1.9517	0.4109	106.466	0.2831	2.3465
K	80	175.32	NaN	NaN	NaN	NaN	NaN	NaN	NaN	0.47999	1.2512	0.1847	69.598	0.1815	1.0545
L	80	211.57	0.56053	0.029	0.0497	81.2978	0.029	0.2836	1.81	0.34177	0.8771	0.0975	49.5571	0.1272	0.5566

WD40A Conductor Shot 6															
Sensor and Charge Data			Measured Data							ARA UWCv2 Data					
Sensor	Sensor Depth Above Mudline (ft)	Slant Range (ft)	Peak Pressure (Mpa)	Impulse (kPa·s)	EFD (kPa·m)	Peak Pressure (PSIpsi)	Impulse (psi·s)	EFD (psi·in)	Time constant (sec)	Peak Pressure (Mpa)	Impulse (kPa·s)	EFD (kPa·m)	Peak Pressure (PSIpsi)	Impulse (psi-s)	EFD (psi-in)
A	5	56.822	0.65409	0.0359	0.0671	94.8672	0.0359	0.3833	1.255	3.09155	7.976	5.5827	448.275	1.1568	31.878
B	45	85.022	0.4643	0.0652	0.0745	67.3409	0.0652	0.4253	1.585	1.49253	3.724	1.4184	216.416	0.5401	8.0991
C	80	115.56	0.81322	-0.003	0.0163	117.948	-0.003	0.0933	0.175	0.85724	2.0851	0.4997	124.3	0.3024	2.8531
D	5	67.868	0.32535	0.0071	0.0067	47.1886	0.0071	0.0383	0.08	2.24264	5.7012	3.0516	325.183	0.8269	17.425
E	45	92.769	0.54259	0.0452	0.0569	78.6967	0.0452	0.3251	2.835	1.27492	3.1581	1.0544	184.864	0.458	6.021
F	80	121.37	0.30109	NaN	NaN	43.6688	NaN	NaN	NaN	0.78448	1.9003	0.4229	113.75	0.2756	2.4146
G	5	84.299	0.22108	0.0108	0.0052	32.0649	0.0108	0.0294	0.99	1.51574	3.7845	1.4602	219.782	0.5489	8.3378
H	45	105.39	0.45104	0.0327	0.0382	65.4177	0.0327	0.2181	1.815	1.01254	2.4817	0.6835	146.818	0.3599	3.9028
I	80	131.27	0.38312	0.0394	0.0314	55.5666	0.0394	0.179	3.315	0.68088	1.6387	0.3239	98.7274	0.2377	1.8497
J	80	147.19	0.29859	0.0286	0.0288	43.3073	0.0286	0.1646	3.44	0.55365	1.3199	0.2195	80.279	0.1914	1.2533
K	80	183.48	NaN	NaN	NaN	NaN	NaN	NaN	NaN	0.37177	0.8702	0.1037	53.9066	0.1262	0.5924
L	80	219.06	0.2586	0.0142	0.0098	37.5065	0.0142	0.056	1.455	0.2699	0.6225	0.0568	39.135	0.0903	0.3243

WD40A Conductor Shot 7															
Sensor and Charge Data			Measured Data							ARA UWCv2 Data					
Sensor	Sensor Depth Above Mudline (ft)	Slant Range (ft)	Peak Pressure (Mpa)	Impulse (kPa·s)	EFD (kPa·m)	Peak Pressure (PSIpsi)	Impulse (psi·s)	EFD (psi·in)	Time constant (sec)	Peak Pressure (Mpa)	Impulse (kPa·s)	EFD (kPa·m)	Peak Pressure (PSIpsi)	Impulse (psi-s)	EFD (psi-in)
A	5	48.016	4.36631	0.1864	2.9816	633.28	0.1864	17.025	1.425	4.98391	14.466	15.091	722.667	2.0981	86.172
B	45	74.199	2.41494	0.0509	0.3984	350.258	0.0509	2.2748	0.005	2.26999	6.355	3.4362	329.148	0.9217	19.621
C	80	104.55	1.13851	0.1251	0.3521	165.127	0.1251	2.0104	2.145	1.22159	3.324	1.0709	177.13	0.4821	6.1149
D	5	63.204	1.31968	0.0576	0.2249	191.403	0.0576	1.2845	1.245	3.03314	8.6053	5.928	439.806	1.2481	33.85
E	45	84.822	2.0312	0.0207	0.1313	294.6	0.0207	0.7496	0.005	1.78248	4.9351	2.1803	258.46	0.7158	12.45
F	80	112.34	2.14055	0.1205	0.4196	310.461	0.1205	2.396	1.835	1.07285	2.9019	0.8388	155.563	0.4209	4.7896
G	5	83.095	1.03333	0.0467	0.1167	149.872	0.0467	0.6665	1.39	1.84999	5.1307	2.3382	268.248	0.7442	13.352
H	45	100.52	2.1257	0.1052	0.6467	308.306	0.1052	3.6927	1.785	1.31144	3.5801	1.2239	190.159	0.5193	6.9886
I	80	124.62	2.14673	0.1141	0.4264	311.356	0.1141	2.4347	1.745	0.88945	2.3852	0.5895	128.97	0.3459	3.3659
J	80	142.92	1.2963	0.0902	0.39	188.012	0.0902	2.2268	2.06	0.69433	1.8409	0.3699	100.678	0.267	2.1122
K	80	182.51	NaN	NaN	NaN	NaN	NaN	NaN	NaN	0.44636	1.1597	0.1611	64.7223	0.1682	0.9198
L	80	220.06	0.88315	0.0387	0.1282	128.09	0.0387	0.7321	1.925	0.31832	0.8143	0.0853	46.1568	0.1181	0.4869

WD40A Conductor Shot 8															
Sensor and Charge Data			Measured Data							ARA UWCv2 Data					
Sensor	Sensor Depth Above Mudline (ft)	Slant Range (ft)	Peak Pressure (Mpa)	Impulse (kPa·s)	EFD (kPa·m)	Peak Pressure (PSIpsi)	Impulse (psi·s)	EFD (psi·in)	Time constant (sec)	Peak Pressure (Mpa)	Impulse (kPa·s)	EFD (kPa·m)	Peak Pressure (PSIpsi)	Impulse (psi-s)	EFD (psi-in)
A	5	36.313	5.48228	0.2694	4.3639	795.137	0.2694	24.918	1.285	6.94296	18.591	25.584	1006.73	2.6963	146.09
B	45	67.221	3.60635	0.2553	1.9522	523.057	0.2553	11.148	2.52	2.28182	5.8054	3.1527	330.864	0.842	18.002
C	80	99.718	2.37975	0.1851	1.0205	345.153	0.1851	5.8274	1.885	1.11892	2.7551	0.8248	162.244	0.3996	4.7099
D	5	52.599	1.17698	0.0306	0.123	170.707	0.0306	0.7025	0.005	3.55451	9.2294	7.259	515.404	1.3386	41.45
E	45	77.244	2.18343	0.1744	1.1616	316.679	0.1744	6.6327	2.33	1.77505	4.4643	1.9654	257.383	0.6475	11.223
F	80	106.73	1.76334	0.1609	0.7142	255.751	0.1609	4.0781	2.625	0.98959	2.4229	0.6546	143.491	0.3514	3.738
G	5	74.061	0.72736	0.0608	0.1244	105.495	0.0608	0.7101	2.25	1.91531	4.8339	2.2678	277.72	0.7011	12.949
H	45	93.193	1.68462	0.1022	0.7827	244.333	0.1022	4.4693	2.77	1.26446	3.131	1.0382	183.347	0.4541	5.9284
I	80	118.79	1.88405	0.142	0.6518	273.258	0.142	3.7217	2.62	0.81562	1.9793	0.455	118.264	0.2871	2.598
J	80	137.07	1.56101	0.1155	0.518	226.406	0.1155	2.958	2.22	0.62973	1.5102	0.2797	91.3108	0.219	1.5969
K	80	177.05	NaN	NaN	NaN	NaN	NaN	NaN	NaN	0.39655	0.931	0.1171	57.4992	0.135	0.6689
L	80	215.07	1.03998	0.0456	0.1845	150.837	0.0456	1.0534	1.875	0.27901	0.6445	0.0605	40.4567	0.0935	0.3452

WD40A Pile Shot 1															
Sensor and Charge Data			Measured Data							ARA UWCv2 Data					
Sensor	Sensor Depth Above Mudline (ft)	Slant Range (ft)	Peak Pressure (Mpa)	Impulse (kPa·s)	EFD (kPa·m)	Peak Pressure (PSIpsi)	Impulse (psi·s)	EFD (psi·in)	Time constant (sec)	Peak Pressure (Mpa)	Impulse (kPa·s)	EFD (kPa·m)	Peak Pressure (PSIpsi)	Impulse (psi-s)	EFD (psi-in)
A	5	121.06	0.65982	0.3443	0.3889	95.6994	0.3443	2.2206	10.995	0.38416	0.6581	0.0905	55.7034	0.0955	0.5166
B	45	135.11	1.72287	0.2685	0.8864	249.881	0.2685	5.0615	4.08	0.33163	0.5607	0.0645	48.0856	0.0813	0.3682
C	80	155.02	3.24148	0.1919	0.98	470.136	0.1919	5.5957	1.845	0.27589	0.4589	0.0422	40.0035	0.0666	0.2411
D	5	142.21	0.4281	0.138	0.3257	62.0902	0.138	1.8599	15.4	0.30966	0.5204	0.0551	44.9	0.0755	0.3145
E	45	154.35	1.34833	0.2083	0.5532	195.559	0.2083	3.1588	4.185	0.27749	0.4618	0.0428	40.2357	0.067	0.2443
F	80	172.04	1.9741	0.1596	0.6719	286.319	0.1596	3.8367	2.36	0.23996	0.3942	0.0306	34.7938	0.0572	0.1749
G	5	163.26	0.26505	0.1511	0.4192	38.4425	0.1511	2.3938	47.515	0.25739	0.4255	0.036	37.3215	0.0617	0.2055
H	45	173.94	1.16883	0.1361	0.3335	169.524	0.1361	1.9041	3.195	0.23646	0.388	0.0296	34.2866	0.0563	0.1691
I	80	189.82	2.42948	0.1407	0.5903	352.366	0.1407	3.3709	1.875	0.21036	0.3416	0.0226	30.5022	0.0495	0.1292
J	80	206.08	1.86851	0.137	0.4791	271.004	0.137	2.7356	2.315	0.18844	0.303	0.0176	27.3233	0.0439	0.1003
K	80	245.27	1.24685	0.0812	0.265	180.84	0.0812	1.5131	1.865	0.14925	0.2351	0.0103	21.6413	0.0341	0.0586
L	80	288.32	0.97512	0.0449	0.1657	141.43	0.0449	0.946	2.04	0.12019	0.1857	0.0062	17.4279	0.0269	0.0356

WD40A Pile Shot 2															
Sensor and Charge Data			Measured Data							ARA UWCv2 Data					
Sensor	Sensor Depth Above Mudline (ft)	Slant Range (ft)	Peak Pressure (Mpa)	Impulse (kPa·s)	EFD (kPa·m)	Peak Pressure (PSIpsi)	Impulse (psi·s)	EFD (psi·in)	Time constant (sec)	Peak Pressure (Mpa)	Impulse (kPa·s)	EFD (kPa·m)	Peak Pressure (PSIpsi)	Impulse (psi-s)	EFD (psi-in)
A	5	89.527	3.65485	0.0679	0.7664	530.091	0.0679	4.3763	0.005	0.57541	1.0218	0.2293	83.4349	0.1482	1.3092
B	45	107.77	4.65467	0.2847	3.2238	675.103	0.2847	18.408	2.075	0.44886	0.7797	0.1294	65.0852	0.1131	0.7391
C	80	131.87	4.54263	0.27	1.9761	658.853	0.27	11.284	1.89	0.34258	0.5809	0.0695	49.6745	0.0843	0.3968
D	5	100.55	1.21294	0.0717	0.1809	175.922	0.0717	1.0332	1.575	0.49255	0.8626	0.1603	71.419	0.1251	0.9153
E	45	117.09	4.36305	0.241	2.193	632.807	0.241	12.522	1.685	0.40169	0.6909	0.1002	58.2444	0.1002	0.5724
F	80	139.59	4.23225	0.2231	1.6395	613.836	0.2231	9.362	1.825	0.31746	0.5347	0.0583	46.0311	0.0776	0.333
G	5	115.39	0.9173	0.4684	0.7688	133.043	0.4684	4.3899	13.205	0.40964	0.7058	0.1049	59.3981	0.1024	0.5989
H	45	130.06	3.59614	0.1814	1.314	521.576	0.1814	7.5029	1.68	0.349	0.5928	0.0725	50.6046	0.086	0.4142
I	80	150.63	4.07666	0.1871	1.507	591.269	0.1871	8.6054	1.685	0.28669	0.4785	0.0461	41.5707	0.0694	0.2634
J	80	162.01	4.16538	0.1693	1.2767	604.138	0.1693	7.29	1.4	0.26006	0.4303	0.0369	37.7085	0.0624	0.2104
K	80	194.39	2.46485	0.118	0.7352	357.497	0.118	4.1981	1.78	0.20375	0.3299	0.021	29.5441	0.0479	0.12
L	80	234.12	2.28405	0.0825	0.4918	331.274	0.0825	2.808	1.44	0.15884	0.2516	0.0118	23.0319	0.0365	0.0677

WD40A Pile Shot 3															
Sensor and Charge Data			Measured Data							ARA UWCv2 Data					
Sensor	Sensor Depth Above Mudline (ft)	Slant Range (ft)	Peak Pressure (Mpa)	Impulse (kPa·s)	EFD (kPa·m)	Peak Pressure (PSIpsi)	Impulse (psi·s)	EFD (psi·in)	Time constant (sec)	Peak Pressure (Mpa)	Impulse (kPa·s)	EFD (kPa·m)	Peak Pressure (PSIpsi)	Impulse (psi-s)	EFD (psi-in)
A	5	51.836	7.99821	0.4571	10.014	1160.04	0.4571	57.181	1.315	1.19607	2.2667	1.2353	173.43	0.3288	7.0539
B	45	79.291	6.3425	0.457	6.3841	919.902	0.457	36.454	1.705	0.677	1.2197	0.3333	98.1657	0.1769	1.9034
C	80	109.83	4.75378	0.0625	0.6679	689.478	0.0625	3.8138	0.205	0.43766	0.7585	0.1221	63.461	0.11	0.6974
D	5	67.735	1.74664	0.9892	3.4524	253.328	0.9892	19.714	14.105	0.83597	1.5346	0.5417	121.216	0.2226	3.0929
E	45	90.487	5.43682	0.3541	4.4467	788.544	0.3541	25.391	2.27	0.56725	1.006	0.2219	82.2517	0.1459	1.2668
F	80	118.17	4.99916	0.3037	2.5925	725.068	0.3037	14.804	2.02	0.39681	0.6818	0.0975	57.5379	0.0989	0.5566
G	5	87.331	1.12372	0.7131	1.7424	162.982	0.7131	9.9493	23.04	0.59487	1.0595	0.2475	86.256	0.1537	1.4133
H	45	105.96	3.64595	0.2463	2.2279	528.8	0.2463	12.722	2.37	0.4592	0.7993	0.1364	66.5842	0.1159	0.7789
I	80	130.39	3.84151	0.2564	2.1406	557.164	0.2564	12.223	2.34	0.3478	0.5906	0.072	50.4314	0.0857	0.4109
J	80	143.45	3.04336	0.2204	1.6383	441.402	0.2204	9.3549	2.59	0.30607	0.5139	0.0536	44.3796	0.0745	0.3062
K	80	178.46	2.34064	0.1238	0.6458	339.481	0.1238	3.6875	0.955	0.22848	0.3738	0.0274	33.1298	0.0542	0.1562
L	80	218.91	1.36596	0.0862	0.2725	198.115	0.0862	1.5563	2.43	0.1738	0.2775	0.0146	25.2007	0.0402	0.0832

WD40A Pile Shot 4															
Sensor and Charge Data			Measured Data							ARA UWCv2 Data					
Sensor	Sensor Depth Above Mudline (ft)	Slant Range (ft)	Peak Pressure (Mpa)	Impulse (kPa·s)	EFD (kPa·m)	Peak Pressure (PSIpsi)	Impulse (psi·s)	EFD (psi·in)	Time constant (sec)	Peak Pressure (Mpa)	Impulse (kPa·s)	EFD (kPa·m)	Peak Pressure (PSIpsi)	Impulse (psi-s)	EFD (psi-in)
A	5	31.166	12.8522	0.6659	20.164	1864.06	0.6659	115.14	1.62	2.36382	4.7592	5.926	342.754	0.6903	33.839
B	45	67.611	7.56311	0.5633	8.3496	1096.94	0.5633	47.678	2.37	0.83802	1.5387	0.5447	121.512	0.2232	3.1103
C	80	101.72	4.31436	0.4222	3.5914	625.745	0.4222	20.507	3.235	0.48501	0.8483	0.1547	70.3264	0.123	0.8834
D	5	51.747	2.189	1.2137	6.4459	317.488	1.2137	36.807	19.89	1.19884	2.2724	1.2419	173.832	0.3296	7.0916
E	45	79.232	6.41817	0.3265	5.5725	930.876	0.3265	31.82	1.82	0.67768	1.221	0.3341	98.2629	0.1771	1.9077
F	80	109.78	4.99632	0.3009	2.932	724.656	0.3009	16.742	2.15	0.43789	0.7589	0.1223	63.4938	0.1101	0.6982
G	5	74.506	3.15863	0.3186	1.9729	458.121	0.3186	11.266	1.105	0.73584	1.3356	0.4038	106.697	0.1937	2.3059
H	45	95.662	4.00124	0.2205	1.6514	580.331	0.2205	9.4299	1.85	0.52655	0.9277	0.1869	76.35	0.1346	1.0673
I	80	122.17	4.43569	0.2321	2.4064	643.342	0.2321	13.741	1.88	0.37948	0.6494	0.0879	55.0249	0.0942	0.5022
J	80	136.1	4.28482	0.1823	1.6698	621.46	0.1823	9.5348	1.525	0.32842	0.5548	0.0631	47.6203	0.0805	0.3601
K	80	171.8	1.98389	0.0062	0.0286	287.739	0.0062	0.1632	0.005	0.2404	0.395	0.0308	34.8586	0.0573	0.1756
L	80	211.28	0.98575	0.0815	0.1972	142.971	0.0815	1.1259	3.12	0.18225	0.2922	0.0163	26.4264	0.0424	0.0928

WD40A Pile Shot 5															
Sensor and Charge Data			Measured Data							ARA UWCv2 Data					
Sensor	Sensor Depth Above Mudline (ft)	Slant Range (ft)	Peak Pressure (Mpa)	Impulse (kPa·s)	EFD (kPa·m)	Peak Pressure (PSIpsi)	Impulse (psi·s)	EFD (psi·in)	Time constant (sec)	Peak Pressure (Mpa)	Impulse (kPa·s)	EFD (kPa·m)	Peak Pressure (PSIpsi)	Impulse (psi-s)	EFD (psi-in)
A	5	87.244	0.75163	0.2316	0.3324	109.014	0.2316	1.8982	6.315	0.59567	1.061	0.2483	86.3716	0.1539	1.4177
B	45	105.88	1.16805	0.1984	0.5745	169.411	0.1984	3.2802	5.125	0.45962	0.8	0.1367	66.6448	0.116	0.7805
C	80	130.33	2.55666	0.2517	1.5022	370.812	0.2517	8.5776	3.23	0.34801	0.591	0.0721	50.4617	0.0857	0.4115
D	5	113.09	0.48518	0.0374	0.0423	70.3689	0.0374	0.2418	1.415	0.42081	0.7268	0.1116	61.0179	0.1054	0.6371
E	45	128.03	1.01397	0.0314	0.1116	147.063	0.0314	0.6373	0.005	0.35644	0.6066	0.0761	51.6831	0.088	0.4348
F	80	148.88	3.06483	0.1661	0.8449	444.516	0.1661	4.8248	1.675	0.29122	0.4868	0.0478	42.2267	0.0706	0.273
G	5	137.44	0.36277	0.2284	0.3797	52.6148	0.2284	2.168	29.285	0.32411	0.5469	0.0612	46.9962	0.0793	0.3493
H	45	149.97	0.78918	0.1158	0.2573	114.461	0.1158	1.4691	4.05	0.28839	0.4816	0.0468	41.8163	0.0699	0.267
I	80	168.13	1.58065	0.1542	0.4167	229.254	0.1542	2.3792	3.08	0.24747	0.4077	0.0329	35.8835	0.0591	0.1877
J	80	186.39	1.46885	0.1187	0.3483	213.039	0.1187	1.9891	3.045	0.21555	0.3508	0.0239	31.2542	0.0509	0.1366
K	80	227.78	0.82593	0.0573	0.182	119.792	0.0573	1.0391	3.105	0.16479	0.2619	0.0129	23.8945	0.038	0.0736
L	80	270.1	0.68046	0.0352	0.1012	98.6927	0.0352	0.5779	2.455	0.13117	0.2043	0.0076	19.02	0.0296	0.0435

WD40A Pile Shot 6															
Sensor and Charge Data			Measured Data							ARA UWCv2 Data					
Sensor	Sensor Depth Above Mudline (ft)	Slant Range (ft)	Peak Pressure (Mpa)	Impulse (kPa·s)	EFD (kPa·m)	Peak Pressure (PSIpsi)	Impulse (psi·s)	EFD (psi·in)	Time constant (sec)	Peak Pressure (Mpa)	Impulse (kPa·s)	EFD (kPa·m)	Peak Pressure (PSIpsi)	Impulse (psi-s)	EFD (psi-in)
A	5	96.578	1.05572	0.0616	0.1784	153.119	0.0616	1.019	1.32	0.51988	0.9149	0.1815	75.382	0.1327	1.0364
B	45	113.7	1.15053	0.0439	0.1185	166.87	0.0439	0.6764	0.99	0.41783	0.7212	0.1098	60.5849	0.1046	0.6268
C	80	136.76	3.23006	0.0955	0.8104	468.481	0.0955	4.6276	0.975	0.3263	0.5509	0.0621	47.3134	0.0799	0.3548
D	5	121.25	0.47091	0.0219	0.0302	68.2992	0.0219	0.1725	0.795	0.38337	0.6566	0.09	55.5884	0.0952	0.5141
E	45	135.28	1.08465	0.0133	0.046	157.315	0.0133	0.2626	0.005	0.33108	0.5597	0.0642	48.0059	0.0812	0.3668
F	80	155.16	2.35756	0.0538	0.2053	341.935	0.0538	1.1721	0.69	0.27554	0.4583	0.0421	39.953	0.0665	0.2404
G	5	144.8	0.48491	0.0169	0.0248	70.3302	0.0169	0.1413	0.835	0.30226	0.5069	0.0521	43.8281	0.0735	0.2975
H	45	156.74	0.78918	0.0311	0.1104	114.461	0.0311	0.6306	0.725	0.27184	0.4516	0.0408	39.4166	0.0655	0.233
I	80	174.19	1.45333	0.033	0.1522	210.787	0.033	0.8692	0.925	0.23601	0.3872	0.0295	34.2209	0.0562	0.1683
J	80	191.83	2.16366	0.0276	0.1198	313.812	0.0276	0.6842	0.415	0.20741	0.3364	0.0219	30.074	0.0488	0.125
K	80	232.84	0.8171	0.0206	0.0456	118.511	0.0206	0.2604	0.705	0.16001	0.2536	0.0121	23.202	0.0368	0.0688
L	80	276.11	0.47079	0.0154	0.0288	68.2821	0.0154	0.1644	0.8	0.12737	0.1978	0.0071	18.4679	0.0287	0.0407

WD40B Pile Shot 1															
Sensor and Charge Data			Measured Data							ARA UWCv2 Data					
Sensor	Sensor Depth Above Mudline (ft)	Slant Range (ft)	Peak Pressure (Mpa)	Impulse (kPa·s)	EFD (kPa·m)	Peak Pressure (PSIpsi)	Impulse (psi·s)	EFD (psi·in)	Time constant (sec)	Peak Pressure (Mpa)	Impulse (kPa·s)	EFD (kPa·m)	Peak Pressure (PSIpsi)	Impulse (psi-s)	EFD (psi-in)
A	5	32.947	12.7547	0.9924	29.988	1849.91	0.9924	171.24	2.61	2.19426	4.3887	4.993	318.168	0.6365	28.511
B	45	68.451	6.6754	0.5505	6.8687	968.185	0.5505	39.221	2.645	0.82428	1.5113	0.5244	119.521	0.2192	2.9943
C	80	102.28	4.35145	0.3493	2.8065	631.125	0.3493	16.025	1.865	0.48146	0.8415	0.1521	69.8113	0.1221	0.8686
D	5	53.467	3.29349	0.1449	1.6575	477.681	0.1449	9.4644	0.005	1.14747	2.1666	1.1228	166.383	0.3142	6.4116
E	45	80.366	4.76048	0.3199	2.7817	690.449	0.3199	15.884	2.235	0.6649	1.196	0.3198	96.4104	0.1735	1.826
F	80	110.61	4.31178	0.2978	2.2472	625.371	0.2978	12.832	2.295	0.43354	0.7507	0.1195	62.8632	0.1089	0.6823
G	5	75.245	2.61631	0.4068	2.3088	379.464	0.4068	13.183	3.52	0.72618	1.3165	0.3917	105.296	0.1909	2.2367
H	45	96.239	3.37477	0.1874	1.4824	489.469	0.1874	8.4646	0.47	0.52233	0.9196	0.1835	75.7377	0.1334	1.0477
I	80	122.62	4.0583	0.2444	1.6963	588.607	0.2444	9.6859	1.985	0.37761	0.6459	0.087	54.7533	0.0937	0.4965
J	80	139.21	3.18978	0.2267	1.3172	462.639	0.2267	7.5212	2.43	0.31861	0.5368	0.0588	46.1979	0.0779	0.3358
K	80	170.06	1.91796	0.1893	0.6678	278.176	0.1893	3.8131	3.245	0.24372	0.401	0.0317	35.3387	0.0582	0.1812
L	80	213.72	1.48393	0.1643	0.4563	215.226	0.1643	2.6056	3.53	0.17947	0.2874	0.0157	26.0233	0.0417	0.0896

WD40B Pile Shot 2															
Sensor and Charge Data			Measured Data							ARA UWCv2 Data					
Sensor	Sensor Depth Above Mudline (ft)	Slant Range (ft)	Peak Pressure (Mpa)	Impulse (kPa·s)	EFD (kPa·m)	Peak Pressure (PSIpsi)	Impulse (psi·s)	EFD (psi·in)	Time constant (sec)	Peak Pressure (Mpa)	Impulse (kPa·s)	EFD (kPa·m)	Peak Pressure (PSIpsi)	Impulse (psi-s)	EFD (psi-in)
A	5	59.709	8.0728	0.5578	11.899	1170.86	0.5578	67.943	2.255	0.98976	1.8444	0.799	143.516	0.2675	4.5622
B	45	84.647	5.54531	0.3209	4.5912	804.279	0.3209	26.216	2.17	0.62026	1.1088	0.2725	89.938	0.1608	1.5561
C	80	113.75	3.87779	0.2493	2.3986	562.426	0.2493	13.697	2.08	0.41755	0.7206	0.1096	60.5443	0.1045	0.6258
D	5	77.623	5.27415	0.2744	3.3224	764.951	0.2744	18.971	1.65	0.69655	1.2581	0.3559	101	0.1825	2.0323
E	45	98.109	4.14938	0.2357	2.8986	601.817	0.2357	16.552	2.39	0.50904	0.8942	0.1729	73.8111	0.1297	0.9874
F	80	124.1	3.57781	0.2153	1.899	518.918	0.2153	10.843	2.305	0.37162	0.6348	0.0838	53.8848	0.0921	0.4786
G	5	97.11	4.80024	0.2607	3.8876	696.216	0.2607	22.199	1.615	0.51606	0.9076	0.1785	74.8287	0.1316	1.019
H	45	114.15	3.64595	0.2314	2.2307	528.8	0.2314	12.737	2.495	0.41561	0.717	0.1084	60.2632	0.104	0.6191
I	80	137.13	3.34139	0.2057	1.6626	484.628	0.2057	9.4935	2.425	0.3251	0.5487	0.0616	47.1395	0.0796	0.3518
J	80	154.64	2.71376	0.211	1.5291	393.597	0.211	8.7312	2.61	0.27678	0.4605	0.0425	40.1329	0.0668	0.2429
K	80	186.03	2.14755	0.1756	0.9894	311.475	0.1756	5.6495	2.745	0.21611	0.3518	0.0241	31.3355	0.051	0.1374
L	80	231.31	2.24547	0.1503	0.7097	325.678	0.1503	4.0525	2.4	0.16143	0.2561	0.0123	23.4078	0.0371	0.0702

WD40B Pile Shot3															
Sensor and Charge Data			Measured Data							ARA UWCv2 Data					
Sensor	Sensor Depth (ft)	Slant Range (ft)	Peak Pressure (Mpa)	Impulse (kPa·s)	EFD (kPa·m)	Peak Pressure (PSI)	Impulse (psi·s)	EFD (psi·in)	Time constant (sec)	Peak Pressure (Mpa)	Impulse (kPa·s)	EFD (kPa·m)	Peak Pressure (PSI)	Impulse (psi-s)	EFD (psi-in)
A	5	99.915	4.60442	0.1102	1.7857	667.815	0.1102	10.197	0.005	0.49675	0.8707	0.1635	72.0293	0.1263	0.9334
B	45	116.55	3.43698	0.0052	0.0744	498.492	0.0052	0.4247	0.005	0.40421	0.6956	0.1017	58.6104	0.1009	0.5807
C	80	139.13	3.27857	0.0058	0.0795	475.516	0.0058	0.4538	0.005	0.31886	0.5373	0.0589	46.2341	0.0779	0.3364
D	5	114.59	3.53665	0.1882	2.1755	512.948	0.1882	12.423	1.19	0.41349	0.713	0.1072	59.9564	0.1034	0.6119
E	45	129.35	2.93588	0.2223	1.5054	425.814	0.2223	8.5961	2.44	0.35157	0.5976	0.0738	50.9782	0.0867	0.4212
F	80	150.02	2.53708	0.181	1.1367	367.972	0.181	6.4905	2.525	0.28827	0.4814	0.0467	41.7989	0.0698	0.2667
G	5	130.91	3.06214	0.2221	2.2692	444.126	0.2221	12.957	2.26	0.34596	0.5872	0.0711	50.1641	0.0852	0.4059
H	45	144	2.34762	0.023	0.1739	340.493	0.023	0.993	0.005	0.3045	0.511	0.053	44.1522	0.0741	0.3026
I	80	162.83	2.87224	0.1986	1.0976	416.583	0.1986	6.2676	2.365	0.25832	0.4272	0.0363	37.4558	0.062	0.2072
J	80	179.96	2.60638	0.2042	1.0173	378.023	0.2042	5.8087	2.745	0.22592	0.3692	0.0267	32.7585	0.0535	0.1522
K	80	210.32	1.78491	0.1758	0.7308	258.88	0.1758	4.173	3.405	0.18336	0.2941	0.0165	26.5873	0.0427	0.0941
L	80	255.48	1.63099	0.1633	0.5611	236.554	0.1633	3.2039	3.275	0.14132	0.2215	0.0091	20.4908	0.0321	0.0517

WD40B Pile Shot4															
Sensor and Charge Data			Measured Data							ARA UWCv2 Data					
Sensor	Sensor Depth (ft)	Slant Range (ft)	Peak Pressure (Mpa)	Impulse (kPa·s)	EFD (kPa·m)	Peak Pressure (PSI)	Impulse (psi·s)	EFD (psi·in)	Time constant (sec)	Peak Pressure (Mpa)	Impulse (kPa·s)	EFD (kPa·m)	Peak Pressure (PSI)	Impulse (psi-s)	EFD (psi-in)
A	5	132.49	1.85898	0.1792	1.0242	269.623	0.1792	5.8481	2.455	0.34046	0.577	0.0685	49.3666	0.0837	0.3912
B	45	145.44	1.43962	0.0582	0.4008	208.799	0.0582	2.2885	1.49	0.30048	0.5037	0.0514	43.5701	0.073	0.2935
C	80	164.1	1.52658	0.0426	0.1193	221.411	0.0426	0.6811	0.49	0.25564	0.4224	0.0354	37.0682	0.0613	0.2023
D	5	155.19	1.0788	0.0628	0.166	156.467	0.0628	0.9478	1.425	0.27547	0.4582	0.0421	39.9429	0.0665	0.2402
E	45	166.39	1.20589	0.0622	0.3454	174.899	0.0622	1.9725	1.3	0.25094	0.4139	0.0339	36.3862	0.06	0.1938
F	80	182.92	0.50901	0.1134	0.1463	73.8251	0.1134	0.8352	5.75	0.22104	0.3605	0.0254	32.0515	0.0523	0.1448
G	5	176.68	1.32648	0.0936	0.2754	192.389	0.0936	1.5723	1.545	0.23156	0.3792	0.0282	33.5765	0.055	0.1611
H	45	186.59	0.83235	0.1012	0.2378	120.722	0.1012	1.3577	2.905	0.21524	0.3502	0.0238	31.2104	0.0508	0.1362
I	80	201.47	1.61621	0.0472	0.1834	234.411	0.0472	1.0472	0.89	0.19423	0.3132	0.0188	28.1628	0.0454	0.1075
J	80	223.21	1.86277	0.0591	0.2069	270.171	0.0591	1.1816	1.065	0.16932	0.2697	0.0137	24.5516	0.0391	0.0784
K	80	258.8	0.70643	0.0847	0.1555	102.459	0.0847	0.888	3.485	0.1389	0.2174	0.0087	20.1404	0.0315	0.0497
L	80	307.13	0.73638	0.0738	0.1498	106.802	0.0738	0.8553	3.09	0.11044	0.1694	0.0051	16.0136	0.0246	0.0293

WD40B Pile Shot 5															
Sensor and Charge Data			Measured Data							ARA UWCv2 Data					
Sensor	Sensor Depth (ft)	Slant Range (ft)	Peak Pressure (Mpa)	Impulse (kPa·s)	EFD (kPa·m)	Peak Pressure (PSI)	Impulse (psi·s)	EFD (psi·in)	Time constant (sec)	Peak Pressure (Mpa)	Impulse (kPa·s)	EFD (kPa·m)	Peak Pressure (PSI)	Impulse (psi-s)	EFD (psi-in)
A	5	105.52	3.03232	0.0506	0.4947	439.801	0.0506	2.8247	0.005	0.46175	0.8041	0.1382	66.9532	0.1166	0.7889
B	45	121.39	1.53598	0.1677	0.533	222.776	0.1677	3.0437	2.695	0.38278	0.6555	0.0897	55.503	0.0951	0.5123
C	80	143.21	0.20259	0.0551	0.0547	29.3835	0.0551	0.3123	9.89	0.30676	0.5151	0.0539	44.4799	0.0747	0.3078
D	5	130.31	0.55596	0.2154	0.2539	80.6345	0.2154	1.4497	11.925	0.3481	0.5911	0.0721	50.4747	0.0857	0.4117
E	45	143.46	1.33093	0.1364	0.508	193.036	0.1364	2.9007	3.32	0.30605	0.5138	0.0536	44.3778	0.0745	0.3061
F	80	162.34	0.56468	0.0737	0.1818	81.8997	0.0737	1.038	9.105	0.25935	0.4291	0.0366	37.6053	0.0622	0.2091
G	5	153.33	0.88676	0.1561	0.3081	128.614	0.1561	1.7596	5.275	0.27997	0.4663	0.0437	40.5955	0.0676	0.2494
H	45	164.65	1.36031	0.0142	0.0495	197.297	0.0142	0.2826	0.005	0.2545	0.4203	0.0351	36.902	0.061	0.2002
I	80	181.34	0.73756	0.1051	0.1806	106.974	0.1051	1.0311	3.35	0.22363	0.3651	0.026	32.4263	0.053	0.1487
J	80	203.35	1.14671	0.096	0.2135	166.317	0.096	1.2191	1.925	0.19182	0.309	0.0183	27.8145	0.0448	0.1044
K	80	239.47	1.04434	0.0733	0.1872	151.469	0.0733	1.0692	2.655	0.15411	0.2434	0.0111	22.3454	0.0353	0.0631
L	80	287.34	1.30222	0.0647	0.1376	188.871	0.0647	0.7856	1.6	0.12074	0.1866	0.0063	17.5077	0.0271	0.036

ARA = Advanced Research Associates Inc.; EFD = energy flux density; in. = inch; kPa = kilopascal; mPa = millipascal; psi = pounds per square inch; s = second; UWCv2 = underwater calculator version 2; WD40A = West Delta Block 40 platform A.

The Department of the Interior Mission

As the Nation's principal conservation agency, the Department of the Interior has responsibility for most of our nationally owned public lands and natural resources. This includes fostering the sound use of our land and water resources; protecting our fish, wildlife, and biological diversity; preserving the environmental and cultural values of our national parks and historical places; and providing for the enjoyment of life through outdoor recreation. The Department assesses our energy and mineral resources and works to ensure that their development is in the best interests of all our people by encouraging stewardship and citizen participation in their care. The Department also has a major responsibility for American Indian reservation communities and for people who live in island communities.

The Bureau of Ocean Energy Management Mission

The Bureau of Ocean Energy Management (BOEM) works to manage the exploration and development of the nation's offshore resources in a way that appropriately balances economic development, energy independence, and environmental protection through oil and gas leases, renewable energy development and environmental reviews and studies.